J Neurophysiol 135: 1480–1498, 2026.
First published May 1, 2026; doi:10.1152/jn.00031.2026

american physiological society

JNP JOURNAL OF NEUROPHYSIOLOGY

RESEARCH ARTICLE

Control of Movement

Spinal mechanisms in postactivation potentiation: facilitation of presynaptic inhibition contrasts H-reflex amplitude reduction

Miloš Kalc,[1,2] Aleš Holobar,[3] Matej Kramberger,[3] Nina Murks,[3] and Jakob Škarabot[2]

[1]*Institute for Kinesiology Research, Science and Research Centre of Koper, Koper, Slovenia;* [2]*School of Sport, Exercise and Health Sciences, Loughborough University, Loughborough, United Kingdom; and* [3]*System Software Laboratory, Faculty of Electrical Engineering and Computer Science, University of Maribor, Maribor, Slovenia*

Abstract

This study investigated the spinal neural mechanisms underlying postactivation potentiation in 10 healthy young males (21.9 ± 4.8 yr). Participants performed a 10-s maximal isometric plantarflexion, after which we measured twitch torque and assessed spinal excitability using the soleus H-reflex, D1 presynaptic inhibition, and heteronymous Ia facilitation (HF). High-density surface EMG was decomposed to track single motor unit responses. The conditioning contraction increased twitch torque by 12.2 Nm ($P < 0.001$) immediately and returned to baseline within 9 min. This mechanical potentiation was accompanied by a 29% reduction in H-reflex amplitude ($P < 0.001$), which recovered within 3 min. Paradoxically, neurophysiological indices of presynaptic inhibition, D1, and HF were significantly increased (D1: $P < 0.017$; HF: $P < 0.001$), resulting in spinal facilitation. Single MU analysis revealed increased discharge probability, particularly in higher-threshold units, indicating overall spinal facilitation. These results demonstrate that postactivation potentiation involves a complex dissociation; H-reflex pathway inhibition along with facilitation of presynaptic spinal mechanisms. This paradox can be explained by either postactivation depression (caused by depletion of neurotransmitter at the Ia-motoneuron synapse) or muscle thixotropy, a contraction history-dependent decrease in muscle spindle sensitivity, which reduces the efficacy of the Ia afferent volley independently of spinal inhibitory mechanisms. Our findings highlight a dissociation between spinal presynaptic facilitation and the decreased H-reflex, underscoring the need for future studies to explicitly test the roles of postactivation depression and muscle thixotropy after conditioning contractions.

NEW & NOTEWORTHY This study provides evidence that postactivation potentiation is accompanied by a reduction in soleus H-reflex amplitude and a concurrent facilitation of presynaptic spinal mechanisms. By combining global EMG and single motor unit analyses extracted from high-density surface EMG, we reveal a dissociation between spinal disinhibition and reflex depression. These findings suggest that acute postcontraction reflex suppression might be mediated by mechanisms other than presynaptic inhibition, potentially involving postactivation depression or changes in muscle spindle sensitivity.

HDsEMG; heteronymous Ia facilitation; Ia afference; soleus; spinal reflex

INTRODUCTION

Muscle contraction history significantly influences subsequent muscle contractions, which can either be enhanced or depressed. For example, electrically elicited tetani or short-lasting (<10 s) voluntary conditioning contractions (1) temporarily increase single-twitch performance. This phenomenon, known as postactivation potentiation (PAP) (2), is primarily influenced by the intensity and duration of the conditioning contraction (1). The principal mechanism behind the observed twitch potentiation is the phosphorylation of the regulatory myosin light chain (3). This phosphorylation alters myosin head orientation, enhancing the likelihood of force-generating cross-bridge interactions by reducing the distance to actin-binding sites (4). As a result, Ca^{2+} sensitivity is increased, making twitch force production more pronounced, particularly at lower contraction intensities, where Ca^{2+} levels are submaximal, and the contractile apparatus is not yet saturated. Indeed, some studies have reported twitch force increases up to 200% immediately following a conditioning contraction (5), with potentiation tapering off exponentially over 10 min.

Correspondence: M. Kalc (milos.kalc@zrs-kp.si); J. Škarabot (j.skarabot@lboro.ac.uk).
Submitted 21 January 2026 / Revised 5 March 2026 / Accepted 28 April 2026

Although the primary mechanisms of PAP are well-established, emerging evidence suggests that neural processes could also contribute (6, 7). However, the precise nature of neural contribution is equivocal, with studies showing Hoffmann reflex (H-reflex) depression (lateral gastrocnemius, LG: 8; soleus, SOL: 9), enhancement (LG: 8; SOL: 8, 10; vastus medialis: 11), or no change (12–14) following a conditioning contraction (see Ref. 3, for a comprehensive review). These discrepancies likely stem from variations in participant characteristics, the nature of the conditioning contractions, time of assessment relative to conditioning contraction, H-reflex assessment methods, muscle selection, and training status [e.g., enhancement more likely shown in trained athletes: Güillich and Schmidtbleicher (8), Folland et al. (11)].

Because reflex potentiation tends to emerge several minutes after a conditioning contraction, while twitch potentiation typically dissipates more rapidly, some have argued that the delayed reflex effects are not directly related to PAP, which mainly contributes to immediate increases in twitch force (15). Instead, they may reflect postactivation performance enhancement (PAPE) (3), which typically arises 5–10 min after a contraction, and encompasses improvements in neuromuscular function not directly linked to myosin regulatory light chain phosphorylation, such as elevated muscle temperature, fluid shifts, or increased blood flow. However, the early H-reflex depression has been linked more closely to PAP and is thought to reflect a compensatory neural strategy, possibly aimed at offsetting the enhanced muscle output (3), but the underlying mechanisms remain experimentally unverified.

A fundamental challenge in interpreting H-reflex changes lies in disentangling presynaptic (e.g., presynaptic inhibition) from postsynaptic (e.g., motoneuron excitability, reciprocal inhibition) mechanisms (16). To address this, electrophysiological techniques often use conditioning stimuli, such as low-intensity volleys to antagonistic nerves, which elicit D1 (5–30 ms) and D2 (70–200 ms) inhibition responses largely attributed to presynaptic inhibition of Ia terminals (17). However, this approach has known limitations: postsynaptic effects may temporally overlap with presynaptic inhibition, while long-latency cutaneous facilitation or shifts in motor unit recruitment thresholds may confound interpretation by mimicking or masking true presynaptic changes (18). To resolve these ambiguities, Hultborn and colleagues (18) demonstrated that, within the first ~0.6 ms of the H-reflex response, monosynaptic Ia excitation remains uncontaminated by disynaptic inputs, making this early window a reliable indicator of pure Ia excitatory postsynaptic potentials (EPSPs). In principle, the most robust way to distinguish changes in presynaptic inhibition from postsynaptic motoneuron recruitment gain is through peristimulus time histogram (PSTH) analysis of single motor unit (MU) discharges, which reflects the direct timing and probability of motoneuron activation in response to synaptic input. Although recent advances in high-density surface electromyography (HDsEMG) decomposition now allow the extraction of single MU responses during evoked contractions (19–22), this approach requires the delivery of a large number of stimuli, typically several tens to construct reliable PSTHs, making it impractical for studies of acute phenomena like PAP, where the time window for capturing spinal adaptations is limited to a few minutes. To address this constraint, we propose to assess the heteronymous Ia femoral facilitation (23, 24), which, in combination with D1 presynaptic inhibition assessment, offers a more time-efficient method that allows a robust indirect quantification of presynaptic inhibitory effects on soleus Ia terminals.

In this study, we aimed to investigate the immediate and short-term neuromuscular responses following a maximal voluntary isometric conditioning contraction. Specifically, we examined the twitch force response and H-reflex amplitude, while also exploring potential contributions from presynaptic spinal mechanisms. Furthermore, leveraging a recently developed methodology to extract single MU discharges from HDsEMG signals in evoked contractions (19, 20, 22), we investigated how MU discharge patterns and amplitude cancellation may influence the observed H-reflex responses. Given the involvement of recreationally active participants in this study, we hypothesized that the conditioning contraction would immediately but transiently increase twitch torque and concurrently decrease the H-reflex amplitude, with reflex responses returning to baseline within approximately 5 min. With respect to presynaptic spinal mechanisms, we further hypothesized that presynaptic inhibition would be reduced following the conditioning contraction, potentially contributing to the observed changes in H-reflex amplitude.

METHODS

Procedures

Participants.

Ten young adult males (age 21.9 ± 4.8 yr) participated in a single-visit counterbalanced crossover repeated-measures study. All participants were physically active at least three times per week with no history of neurological disorders or major lower-extremity neuromuscular injury as determined by a health history questionnaire (Par-Q; 25). Participants were instructed to avoid the consumption of caffeinated beverages and strenuous physical activity 24 h before the experimental session. Each participant was briefed about any potential risks and discomfort they might face, and they provided written informed consent before involvement in the study. This research complied with the most recent principles outlined in the Declaration of Helsinki (except for registration in database), and it received clearance from the Research Ethics Committee of Slovenia (n 0120-84/2020/4).

Study design.

Participants first visited the laboratory for a familiarization session, during which they were acquainted with the electrical stimulation paradigms used in the study. They returned 3–7 days later for the experimental session. The session began with a standardized warm-up consisting of isometric plantarflexion contractions lasting 4–6 s at 50% (2 repetitions), 60% (2x), 70% (1x), 80% (1x), and 90% (1x) of the participant's maximal perceived effort. This was followed by a torque-tracking preliminary procedure (see *Torque tracking preliminary procedure*). Subsequently, stimulation parameters for the tibial, common peroneal, and femoral nerves were determined. A 20-min washout period was then introduced to reduce potential residual effects of the contractions on subsequent measurements.

During the experiment, participants were instructed to remain seated in the ankle dynamometer and perform one of two interventions: *i*) a 10-s maximal voluntary isometric contraction (EXP), or *ii*) passive rest (CON). Following each intervention, mechanical and electrophysiological responses to stimulation were recorded over an 18-min period at 1, 3, 5, 7, 9, 12, 15, and 18 min postintervention. This design, omitting baseline assessments before the intervention, was adapted from previous work (11, 14). A 20-min washout period was included between the two conditions to minimize carryover effects. The warm-up was repeated 10 min before the second intervention. Intervention order was counterbalanced across participants to reduce potential order effects. All testing was conducted in a temperature-controlled room maintained between 22°C and 24°C. A schematic representation of the intervention timeline is shown in Fig. 1*A*.

Participant positioning.

Participants were seated upright in the custom ankle dynamometer with their hips, knees, and ankles flexed at 90° (180° = full extension), consistent with prior studies examining PAP (14). The right leg was used for all measurements. The foot was strapped securely over the metatarsal region onto the footplate, with the lateral malleolus aligned with the device's axis of rotation (Fig. 1*C*). A rigid support was placed over the thigh, just above the knee, to limit unwanted movement during plantarflexion. Participants rested their forearms on the device's arm supports and were instructed to maintain a relaxed posture. To reduce variability in spinal responses, participants were asked to keep their gaze fixed on a monitor in front of them, maintain a neutral head position, and avoid clenching their jaw or squeezing their hands during stimulation (26).

Torque tracking preliminary procedure.

Following the warm-up, participants rested for 60 s before performing two maximal voluntary isometric contractions (MVCs), separated by 120 s of rest. They were instructed to contract as fast and as hard as possible and maintain maximal effort for ~3 s. Strong verbal encouragement was provided to ensure maximal effort (27). After MVC determination, participants completed submaximal isometric contractions lasting 20 s at 10%, 20%, and 30% MVC, and 15 s at 40%, 50%, and 70% MVC. Each contraction was followed by a 120-s rest period to prevent fatigue. These torque-tracking contractions were used to establish MU separation filters, facilitating MU identification during electrically elicited contractions (19, 22), see *HDsEMG processing* for details.

Conditioning contraction.

Participants were instructed to contract their plantar flexors as fast and as hard as possible and maintain maximal effort for 10 s. Strong verbal encouragement was provided to ensure maximal effort (27). As indicated in *Study design*, this was performed after a 20-min washout period following either the torque-tracking preliminary procedure or the other condition (EXP or CON, as per randomization).

Electromyographic recordings.

Electromyographic signals were recorded from the soleus (SOL) muscle using both high-density surface EMG and bipolar EMG (biEMG). Before electrode placement, the skin over the SOL region was shaved and abraded with abrasive paste (28). The electrode array was mounted on the muscle belly covering the central portion of the soleus muscle, with the long side of the array aligned with the longitudinal axis of the muscle (Fig. 1*C*). This electrode position has been suggested as the position where the H-reflex with the largest amplitude can be observed on the soleus muscle (29). The biEMG electrodes were positioned laterally to the array, with a reference electrode positioned over the tibial tuberosity, and a ground electrode wrapped around the ankle. The HDsEMG was used to extract individual motor unit spike trains from both voluntary and evoked contractions, whereas the biEMG setup allowed for real-time monitoring of short signal segments (30 ms before to 70 ms after each electrical stimulus), ensuring visual feedback of the evoked responses and signal quality. The SOL was selected as the target muscle for EMG recordings because it allows for the assessment of multiple spinal inhibitory and facilitatory mechanisms via established H-reflex conditioning protocols (17, 30).

Posterior tibial nerve stimulation.

H-reflexes, M-waves, and mechanical twitches were elicited in the right soleus (SOL) muscle using single rectangular pulses (1-ms duration) delivered to the posterior tibial nerve. The stimulation anode was placed over the patella, while the optimal site for cathodal stimulation in the popliteal fossa was first identified using a stimulation pen and then marked for electrode placement.

To obtain the H-reflex and M-wave (HM) recruitment curve, stimulation began at 5 mA and was progressively increased in 1-mA steps until the maximal H-reflex amplitude (H_{MAX}) was reached. Once the H-reflex began to decline, stimulation intensity was further increased in 5-mA increments until no further increase in M-wave amplitude was observed. To ensure supramaximal stimulation, the final intensity was increased by 50%. These supramaximal stimuli (stimulation current: 92.7 ± 9.9 mA) were used to evoke maximal twitch peak torque (PT) and maximal M-wave (H_{MAX}).

To investigate the different spinal pathways after the interventions, the H-reflex was conditioned with nerve stimulations of homonymous spinal pathways to assess changes in the level of presynaptic inhibition acting on Ia afferent terminals. Unconditioned H-reflexes served as a baseline for conditioned volleys arising from *i*) stimulation of the common peroneal nerve to elicit presynaptic inhibition (D1) and *ii*) stimulation of the heteronymous nerve (femoral nerve) to elicit heteronymous Ia facilitation pathways (HF). In addition, a mini recruitment curve was used to determine changes in maximal H-reflex postintervention. A block of 16 stimuli (Fig. 1*B*), comprising four unconditioned H-reflexes, four stimuli each for assessing D1 and HF, and four with progressively increasing intensity for H_{MAX}, were delivered at 6-s interstimulus intervals (Fig. 1*E*).

Unconditioned H-reflex.

To evoke the unconditioned SOL H-reflexes, the tibial nerve was stimulated with an intensity that induced a response of the SOL H-reflex in the ascending part of the HM recruitment curve (28.1 ± 6.0 mA), preceded by a small visible

M-wave (M_{atH}) of amplitude between 5 and 10% of M_{MAX} (17). The reproducibility of M_{atH} was used to monitor the stability and reliability of the stimulation. A stable M_{atH} indicates that a constant number of motor nerve fibers and Ia afferents are excited by the same stimuli, ensuring the consistency of stimulus condition within the experimental session (31). Thus, the intensity was slightly adjusted during the experiment to elicit a consistent M_{atH} amplitude. The peak-to-peak

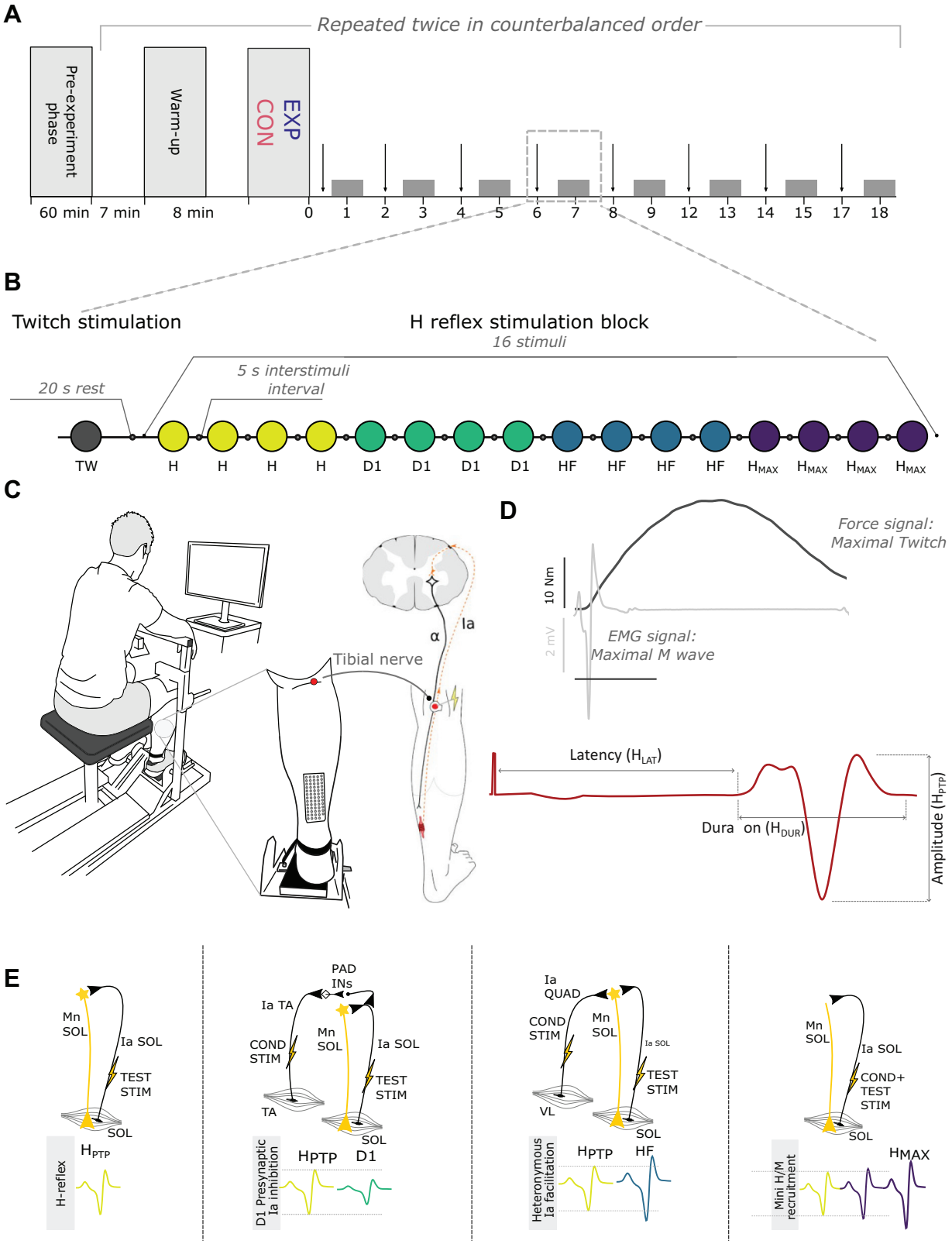

amplitude of the unconditioned H-reflex (H_{PTP}) was further considered in data analysis.

Assessment of D1 presynaptic inhibition.

H-reflexes were conditioned to induce D1 presynaptic inhibition of Ia afferents onto α-motoneurons, following the methodology presented by Knikou (17). Conditioning stimuli, consisting of triplets at 300 Hz (1 ms width), were delivered to the branch of the common peroneal nerve activating the ipsilateral pretibial flexors. Electrical stimulation was delivered with an intensity set at 1.2 times the motor threshold of the tibialis anterior (TA; 32). Optimal conditioning-test timing for maximal H-reflex inhibition was determined for each participant at the start of the session, exploring intervals from 25 ms to 10 ms in 1-ms steps. The timing producing the highest inhibition was used. The ratio between the conditioned (D1) and the unconditioned reflex (H_{PTP}) indicates the activation of presynaptic inhibitory mechanisms (see Fig. 1*D*) and was further considered in data analysis.

Assessment of heteronymous Ia facilitation.

To examine HF, a conditioning stimulus was applied to the ipsilateral femoral nerve (Fig. 1*E*). Single stimulations (1-ms pulse width) were set at 1.3 times the motor threshold of the vastus lateralis muscle. The most effective conditioning test interval for facilitating soleus HF amplitude was identified early in the experimental session, with intervals ranging from −10 ms to +5 ms in 1-ms steps. The timing that produced the highest facilitation in each participant was used. Special attention was given to the conditioning-test interval to ensure monosynaptic interaction of quadriceps Ia afferents with the triceps surae motoneuronal pool (33), as facilitations at larger intervals might also involve polysynaptic circuits. Bergmans et al. (34) have noted that heteronymous Ia facilitation of the H-reflex is not always observable in the lower limbs of all participants. Therefore, only participants who exhibited an increase in SOL H-reflex after a heteronymous conditioning impulse to the femoral nerve in familiarization were invited to participate in the experimental session. The ratio between the conditioned (HF) and the unconditioned reflex (H_{PTP}) indicates the facilitation of the SOL Ia-α motoneuron after femoral nerve activation (18; Fig. 1*D*) and was further considered in data analysis.

Maximal H-reflex amplitude.

The maximal H-reflex was evoked by four stimuli starting at an intensity of 2 mA below the H_{MAX} reached at the beginning of the visit (1-mA increments). The H-reflex response that produced the highest peak-to-peak amplitude (stimulation current: 37.0 ± 9.5 mA) of the series of four stimuli was considered H_{MAX} for that time point.

Stimulation protocol justification.

The stimulation protocol for studying spinal mechanisms in this study involved balancing the need for a sufficiently long interstimuli interval to prevent homosynaptic depression (35) in a resting muscle and the need for a significant number of stimuli to counteract the intrinsic variability of H-reflex amplitude (36). Though longer intervals (~10 s) are crucial to reduce homosynaptic depression risk (35, 37, 38), and 5–10 stimuli are typically needed to obtain a reliable measure of the physiological response (16), we aimed to record as many responses as feasible within a limited timeframe (90 s), targeting 16 stimuli divided into four groups. During the familiarization session, we experimented with shortening the interstimuli interval to determine the shortest possible duration without inducing homosynaptic depression. A 6-s interval emerged as the optimal compromise, as the shortest duration not triggering homosynaptic depression in our participants, thereby allowing for a greater number of stimuli within the given timeframe.

Instrumentation

Isometric dynamometer.

Isometric plantarflexion torque was recorded using a custom-made ankle dynamometer (Wise Technologies, Ljubljana, Slovenia). A load cell (Z6FC3/200 kg, AEP transducers, Modena, Italy) was embedded in the footplate to measure plantarflexion torque.

Electromyography systems.

HDsEMG signals were recorded using a semidisposable adhesive electrode array with 5 columns × 13 rows and 8-mm interelectrode distance (GR08MM1305, OT Bioelettronica, Torino, Italy). Signals were amplified with a 16-bit amplifier (Quattrocento, OT Bioelettronica) and acquired at 5,120 Hz using OTBiolab + software. A reference electrode (5 × 3 cm, T3545) was placed on the tibial tuberosity, and grounding was achieved using a water-soaked strap (WS2, OT Bioelettronica, Torino, Italy) around the ankle. Signals were band-pass filtered between 10 and 500 Hz.

Bipolar EMG signals were recorded with surface electrodes (Covidien 24 mm, interelectrode distance 25 mm) placed lateral to the HDsEMG array. The reference electrode (50 × 100 mm, 00734, Compex, UK) was placed over the patella. Signals were sampled at 10,000 Hz using PowerLab hardware and LabChart software (ADInstruments, Australia) and band-pass filtered (10–500 Hz).

Electrical stimulation equipment.

The posterior tibial nerve was stimulated using a custom-built constant-current stimulator (Stim_1, EMF Furlan, Ljubljana, Slovenia) delivering 1-ms rectangular pulses. The

Figure 1. Study design and schematic representation of the assessment procedures. *A*: study timeline, including the pre-experiment phase and two experimental conditions (EXP and CON). Vertical arrows indicate the timing of supramaximal electrical stimulations, while the gray boxes represent the blocks of stimulation used to assess spinal reflexes. *B*: detailed depiction of the stimulation block, consisting of one supramaximal stimulus (twitch, TW) and 16 submaximal stimuli. These stimuli are grouped in sets of four, designed to assess: H-reflex at the ascending part of the H-M recruitment curve (H), D1 presynaptic Ia inhibition, heteronymous Ia facilitation (HF), and a mini H-M recruitment curve to evaluate the maximal H-reflex. *C*: illustration of the participant's posture on the ankle dynamometer and the points of H-reflex stimulation along the tibial nerve pathway and the placement of the electrode array. *D*: representative examples of mechanical (torque) and electrophysiological (M-wave) responses to a single supramaximal stimulus (upper traces), and a typical H-reflex response to submaximal stimulation (lower trace), with key features extracted from the H-reflex waveform (peak-to-peak amplitude, latency, and duration). *E*: schematic representations of the spinal circuits involved in different types of reflex modulation (from left to right): H-reflex, D1 presynaptic Ia inhibition, heteronymous Ia facilitation, and maximal H-reflex. The corresponding electrophysiological responses are shown for each reflex type.

anode (50 × 90 mm, MyoTrode PLUS, Globus, Italy) was placed over the patella, and the cathode (25 mm diameter, J10R00, Axelgaard) over the popliteal fossa.

The common peroneal and femoral nerves were stimulated using the Digitimer DS7R stimulator (Digitimer, UK). Two silver chloride electrodes (8 mm) were placed over the upper anterolateral leg, distal to the fibular head, to stimulate the common peroneal nerve. For femoral nerve stimulation, the cathode (25 mm diameter, J10R00, Axelgaard Manufacturing Co., Lystrup, Denmark) was placed in the femoral triangle and the anode (50 × 90 mm, MyoTrode PLUS, Globus, Italy) under the gluteus maximus. A manual switch was used to alternate stimulation targets.

Data Processing

Global EMG.

EMG reflex responses were extracted from the array electrode. Two sets of five neighboring monopolar signals within the central portion of the HDsEMG (columns 2–4 and rows 4–7 of the bidimensional array) were averaged and differentiated to obtain a bipolar EMG derivation with an equivalent interelectrode distance of 1.6 cm (39, 40). Although EMG measurements were also taken in a bipolar configuration, we chose to extract the data from the array electrode because the H-reflex amplitude can vary substantially depending on the recording electrode's position (29), and because we aimed to obtain both global EMG and decomposed EMG from the same source.

Maximal M peak-to-peak amplitudes (M_{MAX}) were extracted from supramaximal stimulations. Following recent H-reflex reporting guidelines by Theodosiadou et al. (16), various parameters were extracted from the reflex electrophysiological response, including normalized peak-to-peak amplitude (H_{PTP}/M_{MAX}), reflex latency (H_{LAT}), and duration (H_{DUR}) (Fig. 1*D*). In addition, to study D1 presynaptic inhibition and HF, we calculated the amplitude ratios of D1 and HF conditioned reflexes to their respective unconditioned responses: $D1/H_{PTP}$ and HF/H_{PTP}.

Torque data.

Torque signals were filtered with a low-pass fourth-order zero-lag Butterworth filter at a cutoff frequency of 25 Hz. From these filtered signals, the peak twitch torque (TW_{PT}) was calculated for the supramaximal stimulations.

HDsEMG processing.

An extended explanation of the procedure involved in the detection of single MUs discharges during elicited contractions can be found in our previous works (19, 20, 22). Briefly, HDsEMG signals were decomposed using the well-established convolution kernel compensation (CKC) algorithm (41). First, data from isometric torque tracking contractions collected at the beginning of the experimental session (see *Torque tracking preliminary procedure*) were decomposed for each contraction level in isolation (Fig. 2, *A* and *B*). The decomposition's effectiveness was quantitatively evaluated using the pulse-to-noise ratio (PNR), which is a reliable indicator of the motor unit (MU) identification precision (42). Any MUs with a PNR below 28 dB were excluded from further analysis. The firing patterns of the remaining MUs underwent meticulous scrutiny and refinement by an expert. This editing process involved discarding MUs that exhibited fewer than five consecutive firings, unusually low instantaneous firing rates (<4 Hz), or highly variable firing patterns, as indicated by a coefficient of variation of the interspike interval exceeding 0.4 (43). For each MU that passed these criteria, its respective MU filter was determined. This filter denotes the specific linear combination of spatiotemporal HDsEMG channel data that approximates the spike train of an individual MU (41, 44). Notably, in situations involving isometric muscle contractions, an MU filter derived from signals of one contraction can be applied effectively to signals of another contraction of the same muscle to ascertain the corresponding MU spike train (41, 44). In our experiment, we initially established MU filters from voluntary contraction HDsEMG signals and then applied these filters to the HDsEMG signals of elicited H-reflexes. To avoid redundancy in MU identification across different levels of voluntary contraction, the firing patterns of MUs were compared against each other. Any duplicates identified (i.e., MUs sharing more than 30% of their firings) were removed by retaining only the ones with the highest PNR, thereby ensuring the uniqueness of each MU in the analysis. Subsequently, these refined MU filters were applied to the HDsEMG signals from H-reflexes, facilitating the identification of MU spike trains in evoked contractions (Fig. 2*C*). The identified MU spike trains were segmented into actual MU discharges or baseline noise, an approach inherent to the CKC method (41). The final step involved a meticulous manual review by an expert, who compared the presence of crosstalk in MU spike trains derived from both voluntary and evoked contractions, making manual adjustments to the segmentation results where necessary, as suggested previously (42, 44–46). It is important to note that only MUs identified in the isometric contractions could be detected in electrically evoked contractions. Moreover, recruitment threshold was estimated as the instantaneous torque at the instant of the first spike in the binary spike train during voluntary contractions.

Following MU identification, we extracted the MU firing latencies (HMU_{LAT}, $D1MU_{LAT}$, $HFMU_{LAT}$, and $H_{MAX}MU_{LAT}$) and probability of MU discharge (HMU_{PROB}, $D1MU_{PROB}$, $HFMU_{PROB}$, and $H_{MAX}MU_{PROB}$).

MU discharge ratio was calculated between recognized and discharged MUs for conditioning responses. $D1_{TO}HMU_{RATIO}$ and $HF_{TO}HMU_{RATIO}$ were calculated by subtracting the unconditioned H-reflex discharge ratio from D1 and HF discharge ratios, respectively. This metric was calculated to compare single MU data to $D1/H_{PTP}$ and HF/H_{PTP} extracted from global EMG.

In addition, electrically elicited responses generate MU discharges that are highly synchronous; however, axonal conduction velocities, recruitment thresholds, and the spatial distribution of innervation zones introduce small but systematic differences in MUAP latency (22). MU synchronization was thus quantified using two complementary measures: *1*) the standard deviation of MU firing latencies and *2*) compound motor unit action potential (CMAP) amplitude cancellation. The temporal dispersion of MU discharges was quantified as the standard deviation of MU firing latencies for each reflex response. This measure was computed for all evoked responses (HMU_{SD}, $D1MU_{SD}$, $HFMU_{SD}$, and $H_{max}MU_{SD}$) and reflects the spread of MU discharges around the mean

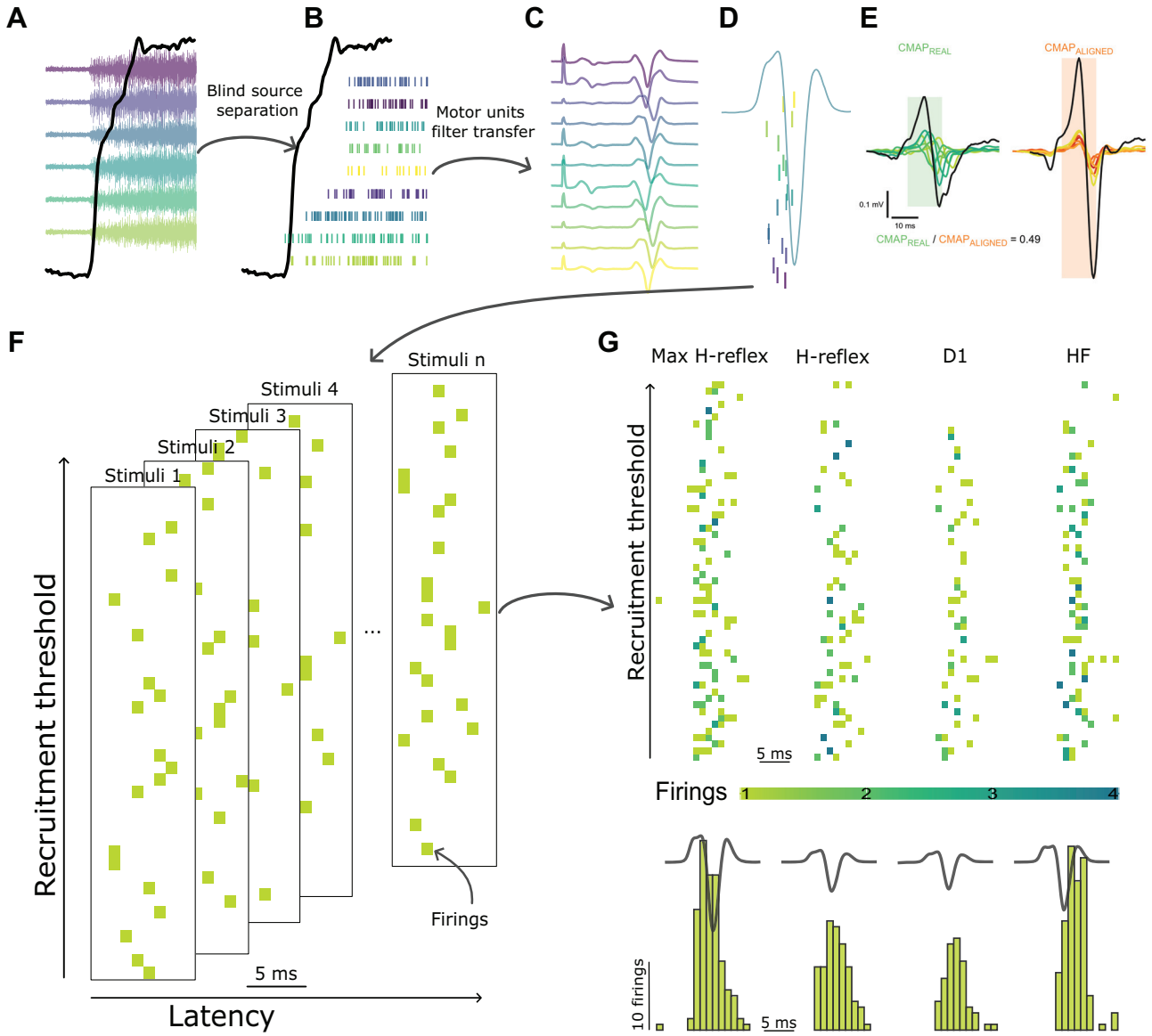

Figure 2. Representative data from a participant and methodological steps to extract single motor unit firings from the HDsEMG recordings. *A*: raw electrophysiological signal during a voluntary isometric contraction. *B*: extracted motor unit firings during voluntary isometric contractions. *C*: reflex response propagation on a sample of channels on an electrode array. *D*: MU firings extracted from a reflex response. *E*: example of CMAP amplitude cancellation. Arithmetic summation of eight MUAPs using recorded latencies and aligned based on the positive peak amplitude, respectively. *F*: graphical representation of MU firings extracted from the electrophysiological response in consecutive stimuli. Each panel represents the temporal distribution (latency) of MUs firings with different recruitment thresholds. *G*: graphical representation of summated MU firings for the maximal H-reflex, H-reflex, D1, and HR responses, respectively. In the *top*, the colored squares represent firing latencies of motor units of different recruitment thresholds. Darker color represents a higher firing count at the same latency at a millisecond precision. The sum of same data is depicted in the histogram at the bottom with the respective global EMG reflex response. Note that the relationship between latencies and recruitment thresholds on the level of individual motor units might not be related, likely due to detection delays (22); however, at the level of the whole sample higher-threshold MUs exhibited longer discharge latencies compared with lower-threshold MUs (see RESULTS).

response latency. CMAP amplitude cancellation arises from the algebraic summation of the positive and negative phases of MUAPs (47) for each reflex response. When MU discharges occur with temporal dispersion, simultaneous summation becomes less constructive, and the resulting compound waveform exhibits a reduced amplitude. Thus, greater cancellation indicates lower synchrony, whereas lower cancellation reflects highly synchronous MU firing (Fig. 2*E*). To quantify cancellation, we computed two versions of the CMAP for each reflex response: $CMAP_{REAL}$, the summation of MUAPs obtained using the actual MU discharge latencies, and $CMAP_{ALIGNED}$, the summation of MUAPs obtained after temporal alignment of all MUAPs at their positive peak, creating an idealized condition of zero temporal dispersion and therefore minimal cancellation. The amplitude cancellation index was then defined in *Eq. 1*:

$$CMAP_{CANC} = \frac{CMAP_{REAL}}{CMAP_{ALIGNED}} \quad (1)$$

Equation 1: $CMAP_{CANC}$ represents CMAP amplitude cancellation, calculated as the ratio between $CMAP_{REAL}$, the arithmetic summation of MUAPS aligned using their true

discharging latencies and $CMAP_{ALIGNED}$ the summation of the same MUPAS aligned at their peak values.

Importantly, although MUAP shape strongly influences amplitude cancellation under typical circumstances (47), this does not pose a methodological limitation here because both $MUAP_{REAL}$ and $MUAP_{ALIGNED}$ are constructed from the same set of MUAPs; therefore, any shape-related factor cancels out, and the ratio isolates only temporal dispersion. However, other limitations of CMAP amplitude cancellation-based metrics may bias the results. Indeed, CMAP amplitude cancellation depends on the number of MU discharges (47). This phenomenon particularly affects the results of this study, because cancellation becomes ill-defined when only one or very few MU discharges are present in a single reflex response, causing the cancellation to approach higher values. We addressed this issue by analyzing the impact of the number of discharging MUs on CMAP amplitude cancellation and reporting our mitigation procedure in the Supplemental Fig. S1.

Please note that the per-MU analyses served as a complementary approach to our primary global EMG analysis. Because meaningful changes in the global EMG were observed only in the early postintervention period, MU-level analyses were restricted to the first four time points.

Statistical Analysis

Statistical analyses were performed using the R programming language (v.4.2.1; R Foundation for Statistical Computing, Vienna, Austria) within the RStudio environment (2025.09.2). Linear and generalized linear mixed-effects models were used to evaluate changes in neurophysiological and mechanical outcomes, with *lme4* (48) and *lmerTest* (49) packages.

To assess the effect of intervention (EXP vs. CON) and time point (eight levels) on torque (TW_{PT}), a set of global EMG outcomes (peak-to-peak amplitude, latency, and duration of reflex responses) and a set of outcomes calculated from the combined discharges of all MUs within each evoked response (MU discharge ratio, MU discharge standard deviation, and CMAP amplitude cancellation), linear mixed-effects models were fitted with intervention, timepoint, and their interaction as fixed effects. Participant IDs were included as random intercepts, with intervention also modeled as a random slope:

$$\text{Outcome} \sim \text{Intervention} \times \text{Timepoint} + (1 + \text{Intervention} \mid \text{Participant ID})$$

MU-level data were extracted only from the first four time points. For MU outcomes based on individual firings (MU discharge probabilities and MU latencies), models were extended to include standardized MU Recruitment Threshold as a continuous covariate. Two-way interactions between Recruitment Threshold and both intervention and time point were included:

$$\text{Outcome} \sim \text{Intervention} \times \text{Timepoint} + \text{Recruitment Threshold} : \text{Intervention} + \text{Recruitment Threshold} : \text{Timepoint} + (1 + \text{Intervention} \mid \text{Participant ID})$$

MU discharge probability, a binary outcome (1 = MU discharged; 0 = MU not discharged), was analyzed using a generalized linear mixed model (GLMM) with a binomial distribution and logit link function in the *lme4* package. Although a logistic link was used, estimated marginal means are reported as predicted probabilities, not odds ratios, to aid interpretation.

Model assumptions (e.g., normality of residuals and random effects, homogeneity of variance, linearity, and multicollinearity) were verified using the performance package (50). All models were analyzed separately for each elicited response condition: H, H_{MAX}, D1, and HF.

Post hoc interaction contrasts and simple effects were tested using the *emmeans* package (51), with P values adjusted using the multivariate t method (52). For torque and global EMG data, the eighth time point was used as the reference level for comparisons; for MU-based data, the fourth time point served as the reference. Estimated marginal means and 95% confidence intervals were reported for all outcomes, while trends of the continuous covariate are presented graphically. The significance threshold for all analyses was set at $\alpha = 0.05$. Cohen's d effect sizes were calculated as the difference between estimated marginal means divided by the residual standard deviation of the fitted model. Effect size thresholds were interpreted as: $d < 0.2$ negligible, $d < 0.5$ small, $d < 0.8$ medium, and $d \geq 0.8$ large (53).

RESULTS

Torque Results

TW_{PT} was significantly affected by time × intervention interaction ($F_{7,\ 146.07} = 27.21$; $P < 0.001$), with interaction contrasts revealing differential modulation of TW_{PT} between interventions at 1, 3, 5, and 7 compared with 18 min after contraction ($P < 0.001$; d = 4.89; $P < 0.001$, d = 2.01; $P < 0.001$, d = 1.85; $P = 0.005$, d = 1.41, respectively) (Fig. 3*C*). Simple contrasts revealed that TW_{PT} in the EXP condition were 12.2 Nm ($P < 0.001$, d = 4.71), 4.73 Nm ($P = 0.002$, d = 1.83), 4.30 Nm ($P = 0.004$, d = 1.66), and 3.18 Nm ($P = 0.028$, d = 1.23) higher compared with CON conditions at 1, 3, 5, and 7 min after intervention, respectively.

Global EMG Results

M_{MAX} was not significantly affected by the interaction between time × intervention ($F_{7,\ 135} = 1.50$, $P = 0.169$, Fig. 3*D*).

H_{PTP}/M_{MAX} was significantly affected by the interaction between time × intervention ($F_{7,\ 496.03} = 3.38$, $P < 0.003$), with interaction contrasts revealing modulation of H_{PTP}/M_{MAX} between interventions at 1 compared with 18 min after contraction ($P = 0.002$; d = 3.60; Fig. 4*D*). Simple contrasts revealed that in H_{PTP}/M_{MAX} in the EXP condition was 29.3 percentage points ($P < 0.001$, d = 3.13) lower compared with CON conditions at 1 min after contraction.

$D1/H_{PTP}$ and HF/H_{PTP} were significantly affected by the interaction between time × intervention ($F_{7,\ 567.13} = 3.70$, $P < 0.001$ and $F_{7,\ 437.33} = 4.99$, $P < 0.001$, respectively), with interaction contrasts revealing modulation in both variables between interventions at 1 compared with 18 min after contraction ($P = 0.017$, d = 0.71, Fig. 4*D*; and $P < 0.001$, d = 1.15, Fig. 4*E*, respectively). Simple contrasts revealed that in $D1/H_{PTP}$ and HF/H_{PTP} in the EXP condition were 17.1 ($P < 0.017$,

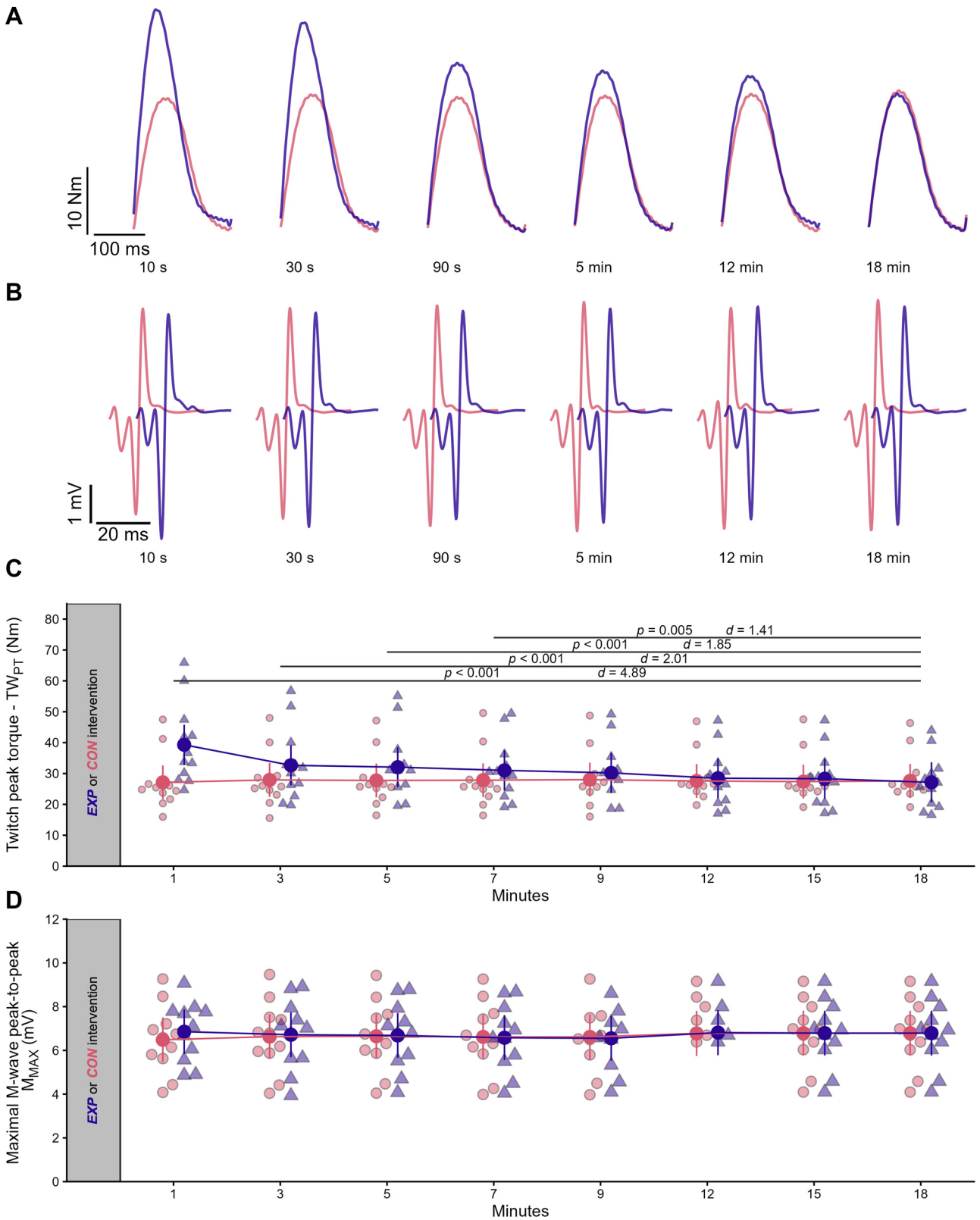

Figure 3. Mechanical and electrophysiological responses to supramaximal electrical stimulations. *A*: torque responses over time from a representative participant, illustrating the modulation of torque traces across different time points. *B*: representative M-wave responses over time. To facilitate comparison between conditions, traces from the EXP condition are time-shifted by 15 ms to avoid overlap. *C*: maximal twitch peak torque across time points. *D*: peak-to-peak M-wave amplitudes (MMAX). Statistical data are presented as estimated marginal means with 95% confidence intervals for both the control (CON, red circles) and experimental (EXP, blue triangles) conditions. Smaller and lighter color circles and triangles represent individual raw data points. Horizontal lines represent statistically significant interaction effects, accompanied by *P* values and Cohen's d values above the relevant lines.

d = 0.57) and 28 percentage points ($P < 0.001$, d = 1.25) higher compared with CON conditions 1 min after intervention. CON condition remained statistically unchanged for the whole duration of the experiment ($P \geq 0.154$).

H_{LAT}, H_{DUR}, and H_{MAX} were not significantly affected by the interaction between time × intervention (H_{LAT}: $F_{6,\ 18.12} = 0.95$, $P = 0.481$; H_{DUR}: $F_{7,\ 64.82} = 0.38$, $P = 0.923$; H_{MAX}: $F_{7,\ 136.00} = 1.45$, $P = 0.190$, Fig. 4*B*; respectively).

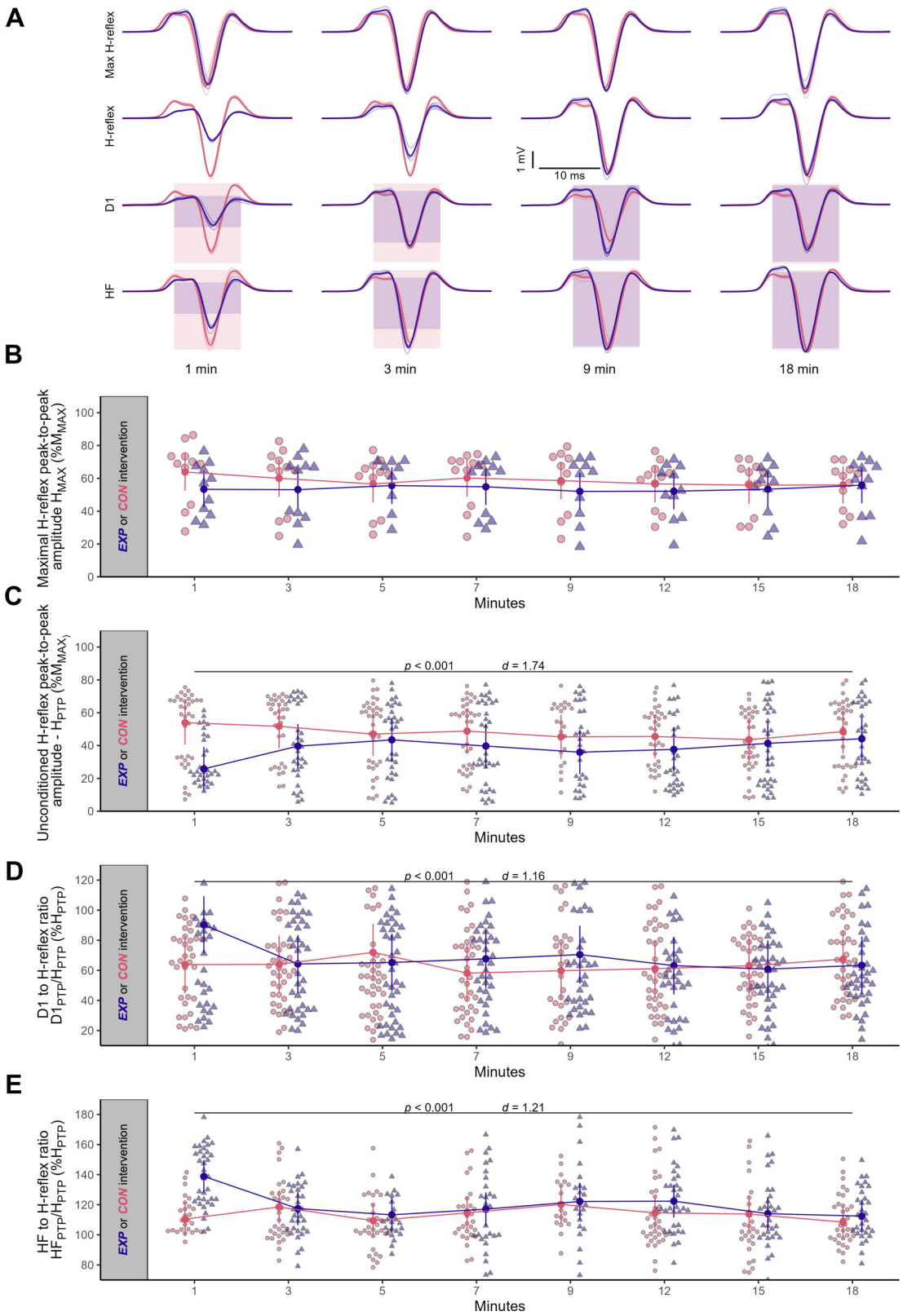

Table 1. *Descriptive statistics of recognized and discharged motor units*

	n	Means ± SD/Person [Range]
Recognized MUs	556	55.6 ± 16.6 [21–78]
Discharged MUs/response		21.8 ± 13.9 [0–64]

Single Motor Unit Behavior Results

A total of 537 MUs resulting in 53.7 ± 16.9 (range 21–78) unique MUs per participant were detected (Table 1). The latencies of MU discharges were not significantly affected by the interaction between time × intervention in any of the assessed conditioning protocols (HMU_{LAT}: $F_{45112.7} = 0.99$, $P = 0.396$; $D1MU_{LAT}$: $F_{3,\ 4573.3} = 1.31$, $P = 0.267$; $HFMU_{LAT}$: $F_{3,\ 5660} = 0.48$, $P = 0.692$; $H_{MAX}MU_{LAT}$: $F_{3,\ 6428.6} = 1.02$, $P = 0.378$; Fig. 5*B*). However, MU discharge latencies were strongly dependent on MU recruitment threshold (HMU_{LAT}: $F_{1,\ 5117} = 21.1$, $P < 0.001$; $D1MU_{LAT}$: $F_{1,\ 4547.3} = 10.49$, $P = 0.001$; $HFMU_{LAT}$: $F_{1,\ 5655} = 34.06$, $P < 0.001$; $H_{MAX}MU_{LAT}$: $F_{1,\ 6426.5} = 29.22$, $P < 0.001$), with higher-threshold MUs exhibiting longer latencies (Fig. 5*C*). Moreover, a significant intervention × recruitment threshold interaction emerged for $D1MU_{LAT}$ ($F_{1,\ 4392.3} = 4.23$, $P = 0.039$), where the EXP condition showed a reduced influence of recruitment threshold on MU firing latency.

MU discharge probability showed a significant interaction between time × intervention in all assessed conditioning protocols (HMU_{PROB}: $\chi^2_3 = 38.09$, $P < 0.001$; $D1MU_{PROB}$: $\chi^2_3 = 27.15$, $P < 0.001$; $HFMU_{PROB}$: $\chi^2_3 = 57.80$, $P < 0.001$; $H_{max}MU_{PROB}$: $\chi^2_3 = 50.04$, $P < 0.001$; Fig. 6*A*). Moreover, a significant intervention × recruitment threshold interaction emerged for all conditioning protocols (HMU_{PROB}: $\chi^2_4 = 206.80$, $P < 0.001$; $D1MU_{PROB}$: $\chi^2_4 = 214.267$, $P < 0.001$; $HFMU_{PROB}$: $\chi^2_4 = 152.67$, $P < 0.001$; $H_{max}MU_{PROB}$: $\chi^2_4 = 115.13$, $P < 0.001$), showing higher probability of MU discharge in higher-threshold MUs in the EXP condition (Fig. 6*B*).

MU discharge ratio was not significantly affected by the interaction between time × intervention in any of the assessed conditioning protocols ($D1_{TO}HMU_{RATIO}$: $F_{3,\ 49.93} = 1.18$, $P = 0.324$; $HF_{TO}HMU_{RATIO}$: $F_{3,\ 50.58} = 1.26$, $P = 0.295$).

CMAP amplitude cancellation for $HCMAP_{CANC}$ and $H_{MAX}CMAP_{CANC}$ were significantly affected by the interaction between time × intervention ($F_{3,\ 205.33} = 3.32$, $P = 0.020$ and $F_{3,\ 157.19} = 4.13$, $P = 0.007$, respectively; Fig. 6*C*). However, interaction contrasts showed no difference between interventions in any time point for $HCMAP_{CANC}$ (Fig. 6*D*), whereas $H_{MAX\text{-}CANC}$ demonstrated a significant difference between 1 and 7 min ($P = 0.008$, d = 0.89). No significant time × intervention interaction was found for $D1_{CANC}$ and HF_{CANC} ($F_{3,\ 163.68} = 0.74$, $P = 0.524$ and $F_{3,\ 224.18} = 2.52$, $P = 0.058$, respectively).

The standard deviation of MU discharges was not significantly affected by the interaction between time × intervention in any of the assessed conditioning protocols (HMU_{SD}: $F_{3,\ 223.15} = 0.49$, $P = 0.687$; $D1MU_{SD}$: $F_{3,\ 217.1} = 2.17$, $P = 0.113$; $HFMU_{SD}$: $F_{3,\ 227} = 0.25$, $P = 0.854$; $H_{max}MU_{SD}$: $F_{1,\ 199.88} = 1.42$, $P = 0.235$) (Fig. 7).

DISCUSSION

This study aimed to investigate the immediate and short-term neuromuscular responses following a maximal voluntary isometric conditioning contraction. Specifically, we assessed the muscle's mechanical (single twitch) and neurophysiological (H-reflex) response, with the aim of elucidating the role of presynaptic spinal mechanisms. The main findings indicate that a brief maximal isometric conditioning contraction led to an increase in twitch torque, accompanied by a diminished H-reflex amplitude, which occurred despite indicators of reduced presynaptic inhibitory spinal mechanisms, as evidenced by increased D1 and HF responses. Modulation of mechanical and neurophysiological responses was transient in nature, vanishing after 9 and 3 min after contraction, respectively. To the best of our knowledge, this is the first study to specifically examine spinal presynaptic mechanisms in the context of PAP.

The Pattern of Mechanical and Neurophysiological Responses Following a Strong Conditioning Contraction

TW_{PT} was increased immediately after the conditioning contraction and persisted for ∼9 min, demonstrating a strong potentiation effect, in line with previous studies investigating PAP (5, 11, 14). Concomitantly, M_{MAX} remained unaffected by any intervention, consistent with a prior study (11), suggesting that sarcolemmal membrane excitability was not affected by the conditioning contraction (54). Conversely, H_{PTP} was significantly decreased immediately following the conditioning contraction, but returned to baseline within 3 min. The decreased H_{PTP} immediately postconditioning contraction is consistent with some studies (8–10) but not others (11, 13, 14), with the discrepancies between studies possibly attributed to variations in training status, conditioning contraction duration, intensity, type, and involved body region, as well as differences in the H-reflex methodology. Regarding the latter, studies interchangeably used the maximal H-reflex and H-reflex measured on the ascending part of the HM recruitment curve (10; like H_{PTP} used in this study). Indeed, in our study, H_{PTP} significantly decreased, whereas the H_{MAX} remained statistically unchanged. Although the lack of observed changes in H_{MAX} might also be due to the timing of the stimulation (i.e., the effect might have

Figure 4. Global electrophysiological responses to submaximal electrical stimulations. *A*: unconditioned (HPTP, HMAX) and conditioned (HD1, HHF) H-reflex responses over time from a representative participant, illustrating the modulation of electrophysiological responses across different time points. Thin line traces represent raw signals; meanwhile, thick traces represent the mean response. Blue and red boxes in D1 and HF traces represent the amplitude of the unconditioned H-reflex in the same stimulation block for EXP and CON interventions, respectively, allowing for a visual comparison of the unconditioned and conditioned H-reflex amplitude. *B*: maximal H-reflex peak-to-peak amplitude (HMAX) across time points. *C*: unconditioned peak-to-peak amplitude of the H-reflex in the ascending part of the H/M recruitment curve (HPTP). *D*: ratio between the conditioned (D1PTP) and unconditioned H-reflex (HPTP) peak-to-peak amplitudes. *E*: ratio between the conditioned (HFPTP) and unconditioned H-reflex (HPTP) peak-to-peak amplitudes. Statistical data are presented as estimated marginal means with 95% confidence intervals for both the control (CON, red circles) and experimental (EXP, blue triangles) conditions. Smaller and lighter color circles and triangles represent individual raw data points in the background. Horizontal lines represent statistically significant interaction effects, accompanied by *P* values and Cohen's d values above the relevant lines.

dissipated by the time H_{MAX} was assessed in our protocol), recent findings suggest that the maximal H-reflex may lack sensitivity to inhibitory mechanisms, potentially obscuring key physiological insights (16).

Prior studies have also reported an increase in reflex amplitude between 4 and 11 min after the contraction (8, 11), an effect not observed in our study. According to a recent review (3), the delayed reflex potentiation reported in some

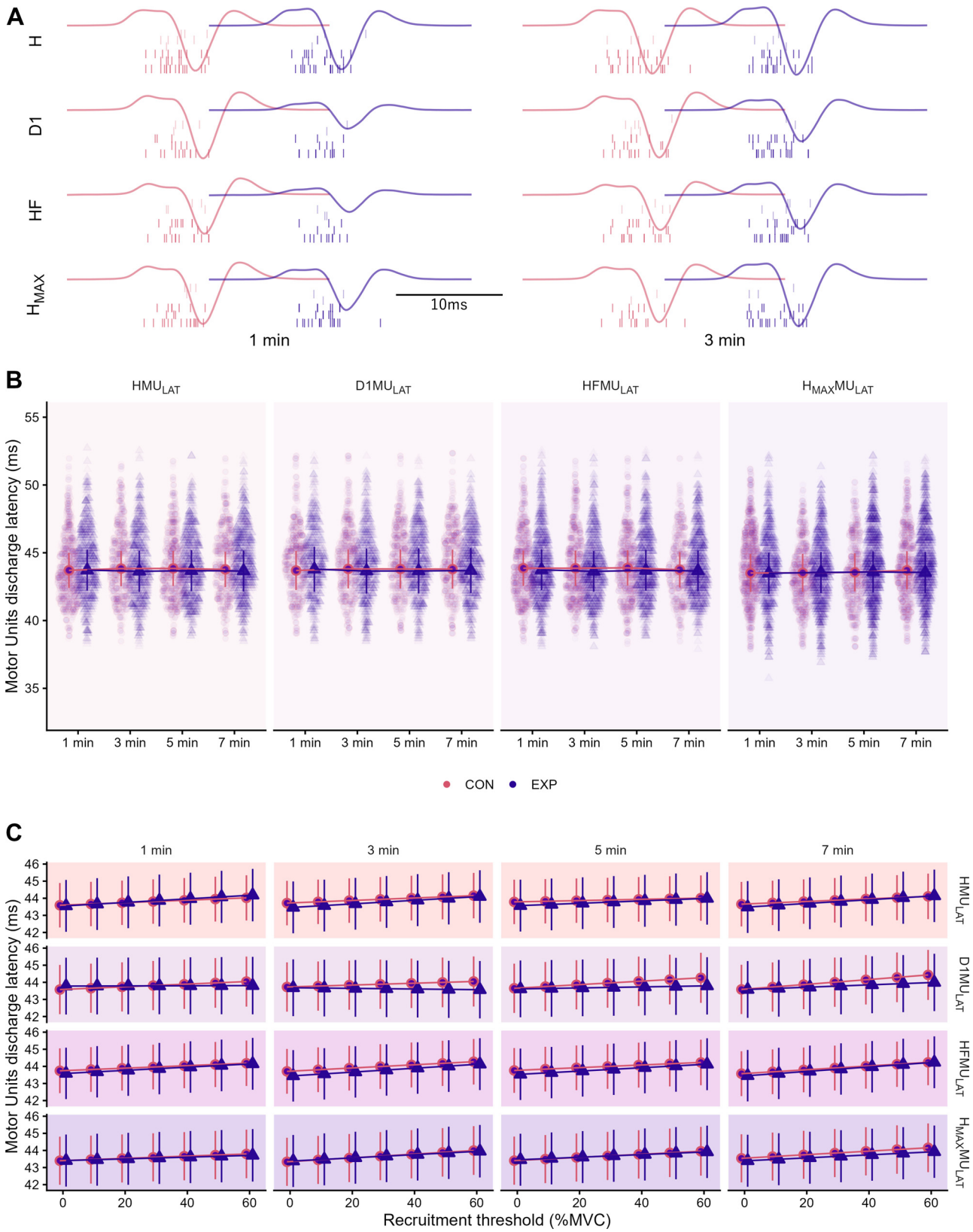

studies might not be attributable to PAP, but to PAPE, a neuromechanical potentiation associated with mechanisms unrelated to PAP, such as increased muscle temperature, water content, and blood flow (15). Furthermore, we can exclude changes in the onset of the reflex responses in the motoneuron or changes in the synchronization of MU firings as the likely mechanisms for the observed H-reflex depression, due to no significant changes in unconditioned and conditioned H-reflex latencies (H_{LAT}); (55) and no differences in the duration of the H-reflex (H_{DUR}), respectively.

In previous studies, the drop in H_{PTP} immediately after conditioning contraction was suggested to be a compensatory mechanism to accommodate the enhanced muscular response (3); however, the direct effect of enhanced muscle contractile properties on the spinal excitability is still unknown. In our data, H_{PTP} amplitude was decreased concomitantly with TW_{PT} increase only at the first time point, suggesting that other mechanisms contribute to the neural modulation observed following the conditioning contraction. Similarly, the acute depression of the H-reflex amplitude is not always found during PAP (12–14).

Moreover, it is important to consider the specific characteristics of SOL when interpreting the relationship between spinal responses and twitch potentiation in the present study. SOL is composed predominantly of slow-twitch muscle fibers (approx. 80%) (56), which are less susceptible to potentiation than fast-twitch fibers (57, 58). Consequently, it is reasonable to suggest that spinal mechanisms associated with PAP in SOL might be less pronounced compared with muscles with a higher proportion of fast-twitch fibers. Furthermore, although the knee was flexed during testing to reduce the mechanical contribution of the gastrocnemius to plantar flexion torque, the tibial nerve stimulation used to elicit twitches and H-reflexes innervates the entire triceps surae. The gastrocnemius muscles, which contain a relatively greater proportion of fast-twitch muscle fibers (approx. 40%) (56), likely contributed substantially to the twitch torque measured, and may therefore account for a considerable portion of the observed potentiation. As such, linking the magnitude of plantar flexor twitch potentiation exclusively to SOL-level spinal adaptations should be interpreted with caution. However, SOL remains the preferred muscle for examining spinal inhibitory and facilitatory mechanisms in humans, providing a methodological window that is not readily available in the gastrocnemius.

The Role of Presynaptic Mechanisms in H-Reflex Reduction Following a Conditioning Contraction

Contrary to our hypothesis, we observed significant increases in presynaptic inhibition-related parameters $D1/H_{PTP}$ and HF/H_{PTP}. Thus, changes of $D1/H_{PTP}$ and HF/H_{PTP} suggest spinal facilitation or disinhibition rather than inhibition. This indicates a complex interplay between inhibitory and facilitatory spinal mechanisms following voluntary contractions and supports the idea that mechanisms other than presynaptic inhibition influence the observed reduction in H_{PTP}. Observations from animal studies show that a short conditioning contraction elevates the transmittance of excitation potentials across synaptic junctions at the spinal cord (36, 59), which can explain the observed disinhibition/facilitation of $D1/H_{PTP}$ and HF/H_{PTP}. An induced tetanic contraction has been suggested to decrease the transmitter failure during subsequent activity, via one or a combination of several possible responses, including an increase in the quantity of neurotransmitter released, an increase in the efficacy of the neurotransmitter, or a reduction in axonal branch-point failure along the afferent neural fibers (59, 60). Moreover, consistent with our findings, following a conditioning contraction in the upper limbs that induced PAP, several studies reported reduced cervicomedullary motor-evoked potential amplitude that has a large monosynaptic component and is generally not influenced by presynaptic inhibition (61, 62).

Another possible explanation for the drop in H_{PTP} observed in our study is the involvement of postactivation depression (PAD), a mechanism often attributed to the depletion of neurotransmitter release at the synaptic cleft due to previous activation of Ia afferents (37). PAD is known to be attenuated during sustained contractions, possibly due to enhanced Ia firing induced by the voluntary contraction (30, 63). In this context, the soleus and gastrocnemius lateralis H-reflex were found to be less depressed immediately after the conditioning contraction when assessed during a sustained voluntary contraction compared with rest, which was interpreted as evidence of PAD-induced depression of the H reflex amplitude (7).

The transient reduction in H_{PTP} observed in the present study could also be explained by a rapid, history-dependent decrease in the sensitivity of muscle spindle Ia afferents, a peripheral phenomenon known as muscle thixotropy (64). After the conditioning contraction, the muscle fibers, having formed stable cross-bridges at a shortened length, would be in a slack state at the testing position. Although the presence of slack in the whole muscle may not always be apparent, the intrafusal fibers of the muscle spindles with their compliant connections to adjacent extrafusal fibers are particularly prone to slack (65), which dramatically reduces tension on the spindle's sensory endings, lowering their baseline discharge rate. This is supported by data in cats, where a conditioning contraction has been shown to dramatically reduce discharge rate of primary muscle spindle endings (from 40 to 10 pps), suggesting a profound, momentary desensitization of the sensory part of the muscle spindle without any change in actual muscle length (66). In the case of our study, the standardized submaximal stimulus that activates the axons originating from spindles will have evoked a less synchronous or less potent volley of action potentials arriving at the spinal cord, leading to weaker excitatory postsynaptic

Figure 5. Motor unit (MU) discharges in elicited contractions. *A*: unconditioned (H, HMAX) and conditioned (D1, HF) H-reflex responses between 1 and 3 min after intervention and respective MU firings from a representative participant. EXP (blue) electrophysiological responses are shifted by 15 ms compared with CON (red) to avoid overlap. Vertical lines represent MU firings. *B*: MU latency across time points. *C*: graphical representation of the influence of recruitment threshold on MU latency across time point and different stimulation conditions. Statistical data are presented as estimated marginal means with 95% confidence intervals for both the control (CON, red circles) and experimental (EXP, blue triangles) conditions. Smaller and lighter color circles and triangles represent individual raw data points in the background. Horizontal lines represent statistically significant interaction effects, accompanied by *P* values and Cohen's d values above the relevant lines.

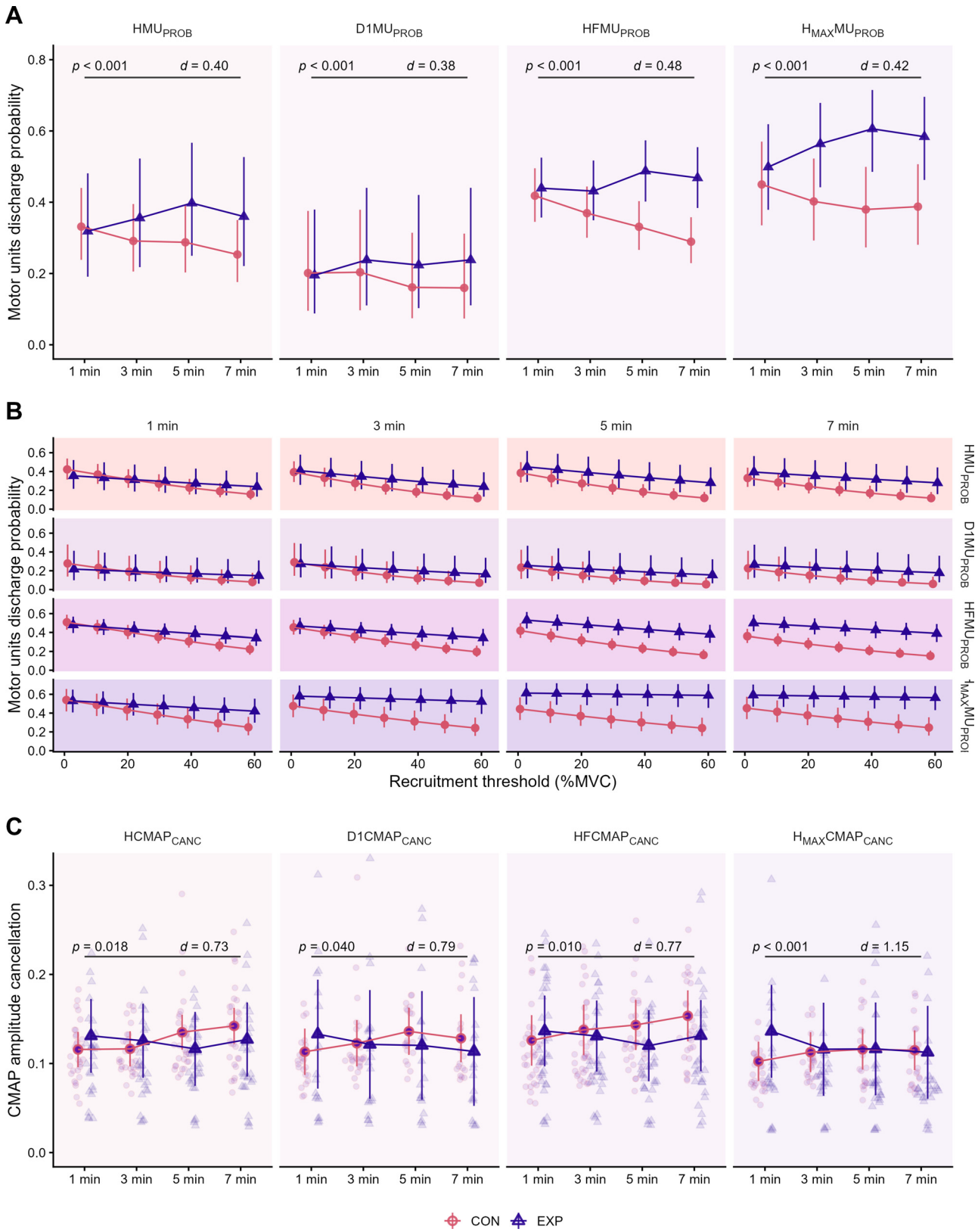

Figure 6. Motor unit (MU) discharges in elicited contractions. *A*: MU discharge probability. *B*: graphical representation of the influence of recruitment threshold on MU discharge probability. *C*: CMAP amplitude cancellation. Statistical data are presented as estimated marginal means with 95% confidence intervals for both the control (CON, red circles) and experimental (EXP, blue triangles) conditions. Smaller and lighter color circles and triangles represent individual raw data points in the background. Horizontal lines represent statistically significant interaction effects, accompanied by *P* values and Cohen's d values above the relevant lines.

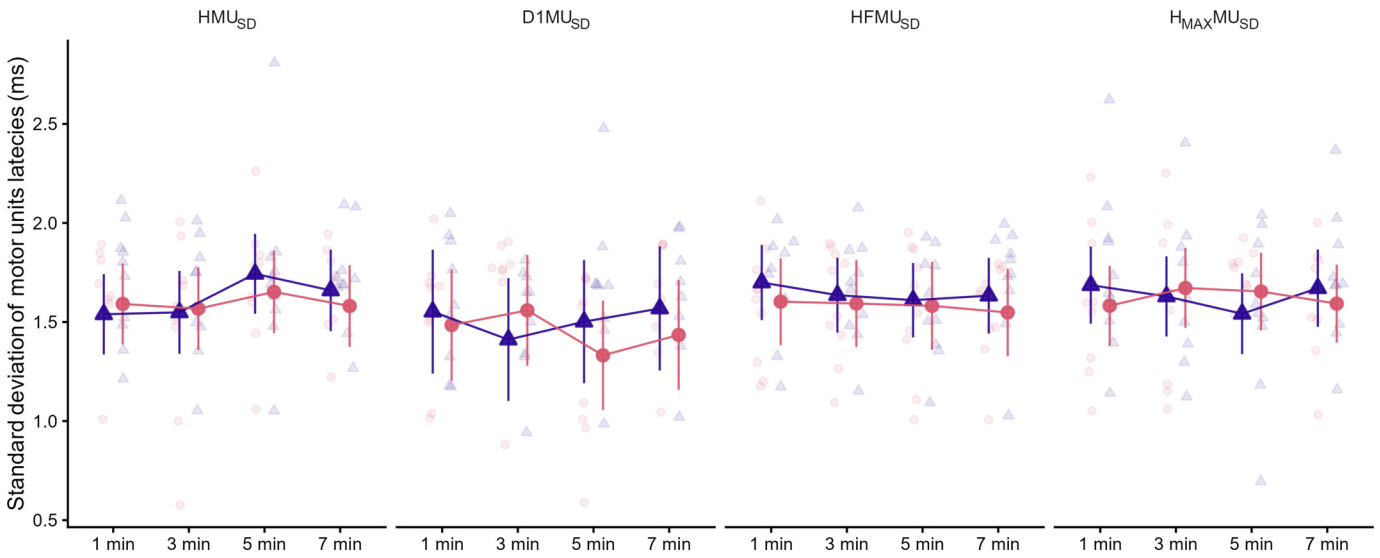

Figure 7. Mean standard deviation of MU firings in elicited contractions. Statistical data are presented as estimated marginal means with 95% confidence intervals for both the control (CON, red circles) and experimental (EXP, blue triangles) conditions. Smaller and lighter color circles and triangles represent individual raw data points in the background.

potential generated by the alpha motoneuron when the spindle axons will have been in a thixotropic, low-sensitivity state after a conditioning contraction, resulting in decreased H-reflex. Indeed, the human evidence supports this supposition, showing that conditioning contractions that alter muscle thixotropy can modulate H-reflex amplitude (67). Although postsynaptic mechanisms such as postactivation depression represent a possible explanation for the apparent contradiction in in our data (i.e., decreased H-reflex with presynaptic inhibition measures pointing toward facilitation), thixotropy offers an additional plausible explanation where the decreased H-reflex reflects a peripheral decrease in Ia-afferent efficacy rather than a change in spinal inhibition. Future studies designed to directly assess postactivation depression and presynaptic inhibition while manipulating muscle thixotropy (e.g., via specific conditioning contractions) are needed to test this hypothesis explicitly.

Effects of a Conditioning Contraction on Spinal Mechanisms Gleaned From Single Motor Units

Additional insights into the effects induced by a conditioning contraction on spinal mechanisms were obtained through the decomposition of the HDsEMG signals into contributions of individual MUs. MU discharge latency was not affected by the conditioning contraction, confirming the results observed from global EMG metrics. Moreover, the MU discharge probability was similar between conditions immediately after the conditioning contraction. However, discharge probability increased 3 min after the contraction in the EXP condition compared with the CON condition across all stimulation paradigms and was significantly higher in higher-threshold MUs. This observation is in line with animal studies where tetanic contraction decreased the transmitter failure occurring primarily at larger motoneurons, which resulted in a considerable potentiation effect in these motoneurons (59). In addition, CMAP amplitude cancellation, a measure of MU discharge synchronization, was lower in the EXP condition, suggesting increased synchronization of MU discharges following the conditioning contraction. Overall, the combination of lower CMAP amplitude cancellation and higher discharge probability, particularly in higher-threshold units, suggests that the conditioning contraction induced facilitation rather than inhibition. These results contradict the reflex amplitude metrics observed at the global EMG level (H_{PTP}), not only in the direction of change but also in timing. Specifically, MU-level differences emerged 3 min after the contraction, whereas the decrease in H_{PTP} occurred immediately. Moreover, these results are in contrast with the observations in studies investigating contraction history effects on voluntary contractions, where an increase in muscle contraction capacity was accompanied by a decrease in MU discharge rate, without clear additional recruitment of MUs to compensate for the discharge rate loss (68, 69).

When interpreting the discrepancy between single MU variables and global EMG metrics reported in this study, it is important to note that MU discharge probability metrics do not represent a fair comparison to $D1_{PTP}/H_{PTP}$ and HF_{PTP}/H_{PTP}, which are normalized to the H_{PTP} amplitude. Thus, we computed the $D1_{TO}H_{RATIO}$ and $HF_{TO}H_{RATIO}$, where we subtracted the number of discharged MUs in the unconditioned contraction from D1 and HF, respectively, and expressed this difference as a ratio with respect to the total identified MUs of each participant. The analysis of the discharge ratio shows that analysis at the MU level also captures the pattern of D1 inhibition and HF facilitation, which can be seen as a decrease or increase in $D1_{TO}H_{RATIO}$ and $HF_{TO}H_{RATIO}$, respectively. However, discharge ratio was not sufficiently sensitive to capture the increase in D1 and HF, as seen in the global EMG ($D1_{PTP}/H_{PTP}$ and HF_{PTP}/H_{PTP}). In this respect, it is important to acknowledge that HDsEMG decomposition captures only a subset of active MUs, with a bias toward larger and more superficial units (45), whereas global EMG provides a more integrated representation of the whole muscle (70). Furthermore, amplitude metrics from global EMG are continuous and nonaffected by single-unit errors, whereas MU-level analyses rely on a relatively small number

of units and discharges. As such, mislabeling or missing a few MU discharges can disproportionately influence the results. Though the single MU analysis provided complementary evidence to increased spinal excitability following voluntary contraction, particularly in higher-threshold units, future studies using a higher stimulus count are warranted to fully exploit the potential of this method for detailed mapping of motoneuron pool adaptations.

The Role of Spinal Mechanisms with Respect to the Reported Effects of Conditioning Contraction on MU Discharge Rate in Submaximal Voluntary Contractions

The increased per-MU discharge probability observed in the present study, derived from H-reflex measures and therefore reflecting the excitability of spinal circuits in response to electrically evoked input, should be contextualized within the broader literature on voluntary MU control when the muscle is in a potentiated state. It has been consistently shown that during voluntary isometric contractions at low-to-moderate intensities (≤75% MVC), MU firing rates are reduced when the muscle is potentiated following a conditioning contraction (68, 69, 71, 72). Interestingly, MU discharge rate is highly responsive to changes in muscle contractile state induced by potentiation and/or sustained contraction, making rapid compensatory discharge rate adjustments (increasing/decreasing discharge rate) dependent on the active state of the muscle. This compensatory mechanism has been speculated to be partially mediated by group III and IV afferents, providing mechanical and metabolic feedback from the muscle to the CNS, as well as by Golgi tendon organs (GTO) conveying tendon tension information via Ib afferents (68, 69). In this regard, musculo-tendinous stiffness has been suggested to increase following a conditioning contraction (see Ref. 15 for a comprehensive review), which could be detected by GTOs and subsequently influence spinal excitability via Ib afferent pathways. However, recent work by Zero and Rice (73) demonstrated that the reduction in voluntary firing rates following a conditioning contraction could be primarily attributable to a decrease in voluntary descending drive rather than to peripheral afferent feedback from the potentiated muscle per se (73). When visual torque feedback was withheld, and participants targeted the same submaximal force level, no modification in MU firing rates or rating of perceived exertion occurred despite the muscle being in a potentiated state; instead, torque output was overestimated by ∼50% (73). This indicates that the motoneuron is not directly sensitized to alterations in the active state of the muscle through peripheral feedback, and that compensatory adjustments in neural output arise from reductions in voluntary descending input driven by visual task demands.

It is therefore important to distinguish between the excitability of spinal circuits as assessed by electrically evoked measures (such as the H-reflex and per-MU discharge probability reported here) and MU discharge behavior during voluntary contractions, which additionally reflects the magnitude of voluntary descending drive and task-specific sensory feedback. Although the present findings suggest that spinal circuitry is in a facilitated state following the conditioning contraction, the net outcome during voluntary submaximal control is a clear reduction in MU firing rates (72). Whether the spinal adaptations reported here (reduced presynaptic inhibition and enhanced heteronymous facilitation) are part of the same compensatory process that permits lower voluntary drive to sustain a given torque output, or represent a distinct and parallel mechanism, remains an open question.

Limitations

This study presents several limitations. First, although the stimulation block intended to induce the H-reflex in the ascending part of the H/M recruitment curve, the D1, HF, and maximal H reflex blocks lasted 90 s, and only four stimuli were elicited per response. Although 5–10 reflexes are typically recommended for reliable assessment (16), the approach used in this study allowed us to examine multiple neurophysiological mechanisms within a single session, with the low variability within each time point (Fig. 4*A*), suggesting four stimuli were sufficient to capture the modulation.

Second, although similar intervals were used in prior work (13), we used a shorter interstimulus interval (6 s) than the 10 s typically recommended for resting H-reflex assessments to minimize postactivation depression (74). Varying intervals were tested during the pilot and familiarization phases, allowing us to identify the shortest interval that did not induce postactivation depression, thereby increasing the number of stimuli per block. Maximal twitches were elicited immediately after the conditioning contraction and could theoretically influence subsequent H reflexes. However, an identical stimulation paradigm was used in the CON condition, which did not show any decrease in H-reflex amplitude, suggesting that prior maximal stimulations did not bias the reflex responses. The maximal H-reflex was assessed 60 s after H_{PTP}, which may have allowed conditioning contraction-induced modulation to dissipate. Nonetheless, HF assessed just 20 s earlier remained significantly elevated, suggesting that the absence of H_{MAX} modulation more likely reflects a methodological limitation of H_{MAX}, rather than an absence of neurophysiological effects.

Furthermore, this study was conducted exclusively in males. Sex hormones fluctuate across the menstrual cycle and are known to modulate spinal excitability (75), and H-reflex parameters have been shown to differ between sexes even when hormone levels are comparable (76). Caution should therefore be exercised when generalizing these findings to female populations or to individuals experiencing hormonal changes across the lifespan. Future studies should examine whether the present findings extend to females.

MU-level analysis is biased by the small number of units identifiable within each evoked response. Although our group has previously demonstrated the feasibility of extracting MUs from evoked responses (19, 20, 22), achieving physiologically robust results still requires hundreds of responses. For example, in a recent study (21), we successfully used PSTHs to extract information from the earliest portion of the reflex response, which reflects the monosynaptic phase of Ia presynaptic inhibition (18). Although this analysis reinforced the physiological effects observed at the global EMG level, a greater number of evoked responses than the number used in the present study is required for HDsEMG-derived MU metrics to reach the reliability comparable to intramuscular EMG. Future attempts to apply similar techniques to study fast, transient neurophysiological phenomena, such as PAP should consider incorporating low-intensity background

muscle activity to reduce postactivation depression (a common limitation in resting H-reflex paradigms) and enable the acquisition of a much greater number of stimuli within a similar assessment window. This approach would strengthen the robustness of noninvasive spinal assessments and enhance the mechanistic insights available from PSTH/PSF analyses.

Finally, it is important to acknowledge that a maximal voluntary conditioning contraction may simultaneously induce contractile dysfunction alongside potentiation (77). These two processes share a common Ca^{2+} dependency but operate through opposing mechanisms. Activity-dependent potentiation results from phosphorylation of the RLC, which increases the Ca^{2+} sensitivity of the contractile apparatus, enhancing force production at submaximal Ca^{2+} concentrations without altering maximal force (78, 79). Contractile dysfunction as a result of a sustained contraction, by contrast, is primarily associated with a reduction in peak myoplasmic Ca^{2+} concentration due to inhibited release from the sarcoplasmic reticulum, impairing force production particularly at high frequencies (80) or decreased Ca^{2+} sensitivity (81). Because potentiation preferentially enhances force at low-stimulation frequencies (single twitch), while contraction-induced contractile dysfunction impairs force at high frequencies (doublet or train), these two processes can coexist with opposing effects at different points along the force-frequency relationship. However, our postconditioning assessment relied exclusively on single electrically elicited twitches and H-reflexes, and thus any contractile dysfunction-related impairment at higher stimulation frequencies would not have been detectable with the methodology used. Although previous studies using a similar conditioning contraction reported no contractile dysfunction (68), whether the observed twitch potentiation reflects pure potentiation or a net outcome of coexisting potentiation and contraction-induced contractile dysfunction therefore remains unresolved. Future studies should incorporate a proper stimulations methodology to dissociate these effects.

Conclusions

This study offers novel insights into the neuromuscular responses following a maximal voluntary isometric conditioning contraction, particularly regarding spinal mechanisms. Our results indicate that a brief but intense voluntary contraction enhances twitch torque, accompanied by a disinhibition (facilitation) of presynaptic inhibitory mechanisms, as shown by increased D1 and HF responses. The observed reduction in H-reflex amplitude immediately after the contraction, however, suggests that additional spinal mechanisms or an intrinsic muscle contraction history-dependent mechanical state may modulate spinal output. Future studies should therefore dissociate spinal mechanisms from muscle thixotropy using protocols that isolate their independent effects.

DATA AVAILABILITY

Data will be made available upon reasonable request.

SUPPLEMENTAL MATERIAL

Supplemental Fig. S1: https://doi.org/10.17605/OSF.IO/78CDW.

GRANTS

M. Kalc was supported by the Sloveniana Research and Innovation Agency (projects: J2-1731, MN-0036; programme: P5-0381). A.H., M. Kramberger, and N.M. were supported by the European Union's Horizon Europe Research and Innovation Program (HybridNeuro project, GA No. 101079392) and by the Slovenian Research and Innovation Agency (project: J2-1731; programme P2-0041). Views and opinions expressed are however those of the author(s) only and do not necessarily reflect those of the European Union or Research Executive Agency. Neither the European Union nor the granting authority can be held responsible for them.

DISCLOSURES

No conflicts of interest, financial or otherwise, are declared by the authors.

AUTHOR CONTRIBUTIONS

M. Kalc, A.H., and J.Š. conceived and designed research; M. Kalc, and M. Kramberger performed experiments; M. Kalc, A.H., and N.M. analyzed data; M. Kalc, and J.Š. interpreted results of experiments; M. Kalc prepared figures; M. Kalc drafted manuscript; M. Kalc, A.H., and J.Š. edited and revised manuscript; M. Kalc, A.H., M. Kramberger, N.M., and J.Š. approved final version of manuscript.

REFERENCES

1. **Vandervoort AA**, **Quinlan J**, **McComas AJ.** Twitch potentiation after voluntary contraction. *Exp Neurol* 81: 141–152, 1983. doi:10.1016/0014-4886(83)90163-2.
2. **Sale DG.** Postactivation potentiation: role in human performance. *Exerc Sport Sci Rev* 30: 138–143, 2002. doi:10.1097/00003677-200207000-00008.
3. **Zero AM**, **Rice CL.** State-of-the-art review: spinal and supraspinal responses to muscle potentiation in humans. *Eur J Appl Physiol* 121: 1271–1282, 2021. doi:10.1007/s00421-021-04610-x.
4. **Levine RJ**, **Kensler RW**, **Yang Z**, **Stull JT**, **Sweeney HL.** Myosin light chain phosphorylation affects the structure of rabbit skeletal muscle thick filaments. *Biophys J* 71: 898–907, 1996. doi:10.1016/S0006-3495(96)79293-7.
5. **Baudry S**, **Duchateau J.** Postactivation potentiation in human muscle is not related to the type of maximal conditioning contraction. *Muscle Nerve* 30: 328–336, 2004. doi:10.1002/mus.20101.
6. **Tillin NA**, **Bishop D.** Factors modulating post-activation potentiation and its effect on performance of subsequent explosive activities. *Sports Med* 39: 147–166, 2009. doi:10.2165/00007256-200939020-00004.
7. **Xenofondos A**, **Patikas D**, **Koceja DM**, **Behdad T**, **Bassa E**, **Kellis E**, **Kotzamanidis C.** Post-activation potentiation: The neural effects of post—activation depression. *Muscle Nerve* 52: 252–259, 2015. doi:10.1002/mus.24533.
8. **Güllich A**, **Sehmidtbleicher D.** MVC-induced short-term potentiation of explosiv force. *New Studies in Athletics* 11: 67–84, 1996.
9. **Enoka RM**, **Hutton RS**, **Eldred E.** Changes in excitability of tendon tap and Hoffmann reflexes following voluntary contractions. *Electroencephalogr Clin Neurophysiol* 48: 664–672, 1980. doi:10.1016/0013-4694(80)90423-x.
10. **Trimble MH**, **Harp SS.** Postexercise potentiation of the H-reflex in humans. *Med Sci Sports Exerc* 30: 933–941, 1998. doi:10.1097/00005768-199806000-00024.
11. **Folland JP**, **Wakamatsu T**, **Fimland MS.** The influence of maximal isometric activity on twitch and H-reflex potentiation, and quadriceps femoris performance. *Eur J Appl Physiol* 104: 739–748, 2008. doi:10.1007/s00421-008-0823-6.
12. **Hodgson MJ**, **Docherty D**, **Zehr EP.** Postactivation potentiation of force is independent of h-reflex excitability. *Int J Sports Physiol Perform* 3: 219–231, 2008. doi:10.1123/ijspp.3.2.219.

13. **Iglesias-Soler E**, **Paredes X**, **Carballeira E**, **Márquez G**, **Fernández-Del-Olmo M.** Effect of intensity and duration of conditioning protocol on post-activation potentiation and changes in H-reflex. *Eur J Sport Sci* 11: 33–38, 2011. doi:10.1080/17461391003770517.
14. **Wallace BJ**, **Shapiro R**, **Wallace KL**, **Abel MG**, **Symons TB.** Muscular and neural contributions to postactivation potentiation. *J Strength Cond Res* 33: 615–625, 2019. doi:10.1519/jsc.0000000000003011.
15. **Blazevich AJ**, **Babault N.** Post-activation potentiation versus post-activation performance enhancement in humans: historical perspective, underlying mechanisms, and current issues. *Front Physiol* 10: 1359, 2019. doi:10.3389/fphys.2019.01359.
16. **Theodosiadou A**, **Henry M**, **Duchateau J**, **Baudry S.** Revisiting the use of Hoffmann reflex in motor control research on humans. *Eur J Appl Physiol* 123: 695–710, 2023. doi:10.1007/s00421-022-05119-7.
17. **Knikou M.** The H-reflex as a probe: pathways and pitfalls. *J Neurosci Methods* 171: 1–12, 2008. doi:10.1016/j.jneumeth.2008.02.012.
18. **Hultborn H**, **Meunier S**, **Morin C**, **Pierrot-Deseilligny E.** Assessing changes in presynaptic inhibition of I a fibres: a study in man and the cat. *J Physiol* 389: 729–756, 1987. doi:10.1113/jphysiol.1987.sp016680.
19. **Kalc M**, **Skarabot J**, **Divjak M**, **Urh F**, **Kramberger M**, **Vogrin M**, **Holobar A.** Identification of motor unit firings in H-reflex of soleus muscle recorded by high-density surface electromyography. *IEEE Trans Neural Syst Rehabil Eng* 31: 119–129, 2023. doi:10.1109/TNSRE.2022.3217450.
20. **Kalc M**, **Skarabot J**, **Divjak M**, **Urh F**, **Kramberger M**, **Vogrin M**, **Holobar A.** Motor unit identification in the M waves recorded by high-density electromyogram. *IEEE Trans Biomed Eng* 70: 1662–1672, 2023. doi:10.1109/TBME.2022.3224962.
21. **Magdič M**, **Holobar A**, **Kramberger M**, **Vogrin M**, **Murks N**, **Fekonja A**, **Kalc M.** Acute effects of orofacial, neck, and shoulder relaxation exercises and chewing on soleus H-reflex and motor unit discharge patterns. *J Neurophysiol* 133: 1886–1901, 2025. doi:10.1152/jn.00461.2024.
22. **Škarabot J**, **Ammann C**, **Balshaw TG**, **Divjak M**, **Urh F**, **Murks N**, **Foffani G**, **Holobar A.** Decoding firings of a large population of human motor units from high-density surface electromyogram in response to transcranial magnetic stimulation. *J Physiol* 601: 1719–1744, 2023. doi:10.1113/JP284043.
23. **Grosprêtre S**, **Gueugneau N**, **Martin A**, **Lepers R.** Presynaptic inhibition mechanisms may subserve the spinal excitability modulation induced by neuromuscular electrical stimulation. *J Electromyogr Kinesiol* 40: 95–101, 2018. doi:10.1016/j.jelekin.2018.04.012.
24. **Pierrot-Deseilligny E**, **Mazevet D.** The monosynaptic reflex: a tool to investigate motor control in humans. Interest and limits. *Neurophysiol Clin* 30: 67–80, 2000. doi:10.1016/s0987-7053(00)00062-9.
25. **Thomas S**, **Reading J**, **Shephard RJ.** Revision of the physical activity readiness questionnaire (PAR-Q). *Can J Sport Sci* 17: 338–345, 1992.
26. **Mitsuyama A**, **Takahashi T**, **Ueno T.** Effects of teeth clenching on the soleus H reflex during lower limb muscle fatigue. *J Prosthodont Res* 61: 202–209, 2017. doi:10.1016/j.jpor.2016.05.003.
27. **Verges S**, **Maffiuletti N A**, **Kerherve H**, **Decorte N**, **Wuyam B**, **Millet GY.** Comparison of electrical and magnetic stimulations to assess quadriceps muscle function. *J Appl Physiol (Bethesda)* 106: 701–710, 2009. doi:10.1152/japplphysiol.01051.2007.
28. **Piervirgili G**, **Petracca F**, **Merletti R.** A new method to assess skin treatments for lowering the impedance and noise of individual gelled Ag-AgCl electrodes. *Physiol Meas* 35: 2101–2118, 2014. doi:10.1088/0967-3334/35/10/2101.
29. **Botter A**, **Vazzoler I**, **Vieira TM.** High density EMG investigation of h-reflex distribution over the soleus muscle. *Annu Int Conf IEEE Eng Med Biol Soc* 2015: 3460–3463, 2015. doi:10.1109/EMBC.2015.7319137.
30. **Burke D.** Clinical uses of H reflexes of upper and lower limb muscles. *Clin Neurophysiol Pract* 1: 9–17, 2016. doi:10.1016/j.cnp.2016.02.003.
31. **Grosprêtre S**, **Papaxanthis C**, **Martin A.** Modulation of spinal excitability by a sub-threshold stimulation of M1 area during muscle lengthening. *Neuroscience* 263: 60–71, 2014. doi:10.1016/j.neuroscience.2014.01.013.
32. **Achache V**, **Roche N**, **Lamy J-C**, **Boakye M**, **Lackmy A**, **Gastal A**, **Quentin V**, **Katz R.** Transmission within several spinal pathways in adults with cerebral palsy. *Brain* 133: 1470–1483, 2010. doi:10.1093/brain/awq053.
33. **Morita H**, **Shindo M**, **Yanagawa S**, **Yoshida T**, **Momoi H**, **Yanagisawa N.** Progressive decrease in heteronymous monosynaptic Ia facilitation with human ageing. *Exp Brain Res* 104: 167–170, 1995. doi:10.1007/BF00229867.
34. **Bergmans J**, **Delwaide PJ**, **Gadea-Ciria M.** Short-latency effects of low-threshold muscular afferent fibers on different motoneuronal pools of the lower limb in man. *Exp Neurol* 60: 380–385, 1978. doi:10.1016/0014-4886(78)90091-2.
35. **Özyurt MG**, **Topkara B**, **Şenocak BS**, **Budan AS**, **Yüce MN**, **Türker KS.** Post-activation depression of primary afferents reevaluated in humans. *J Electromyogr Kinesiol* 54: 102460, 2020. doi:10.1016/j.jelekin.2020.102460.
36. **Gossard JP**, **Floeter MK**, **Kawai Y**, **Burke RE**, **Chang T**, **Schiff SJ.** Fluctuations of excitability in the monosynaptic reflex pathway to lumbar motoneurons in the cat. *J Neurophysiol* 72: 1227–1239, 1994. doi:10.1152/jn.1994.72.3.1227.
37. **Hultborn H**, **Illert M**, **Nielsen J**, **Paul A**, **Ballegaard M**, **Wiese H.** On the mechanism of the post-activation depression of the H-reflex in human subjects. *Exp Brain Res* 108: 450–462, 1996. doi:10.1007/bf00227268.
38. **Stein RB**, **Estabrooks KL**, **McGie S**, **Roth MJ**, **Jones KE.** Quantifying the effects of voluntary contraction and inter-stimulus interval on the human soleus H-reflex. *Exp Brain Res* 182: 309–319, 2007. doi:10.1007/s00221-007-0989-x.
39. **Del Vecchio A**, **Negro F**, **Felici F**, **Farina D.** Associations between motor unit action potential parameters and surface EMG features. *J Appl Physiol (1985)* 123: 835–843, 2017. doi:10.1152/japplphysiol.00482.2017.
40. **Del Vecchio A**, **Negro F**, **Felici F**, **Farina D.** Distribution of muscle fibre conduction velocity for representative samples of motor units in the full recruitment range of the tibialis anterior muscle. *Acta Physiol (Oxf)* 222: e12930, 2018. doi:10.1111/apha.12930.
41. **Holobar A**, **Zazula D.** Multichannel blind source separation using convolution kernel compensation. *IEEE Trans Signal Process* 55: 4487–4496, 2007. doi:10.1109/TSP.2007.896108.
42. **Holobar A**, **Farina D**, **Gazzoni M**, **Merletti R**, **Zazula D.** Estimating motor unit discharge patterns from high-density surface electromyogram. *Clin Neurophysiol* 120: 551–562, 2009. doi:10.1016/j.clinph.2008.10.160.
43. **Drost G**, **Stegeman DF**, **van Engelen BGM**, **Zwarts MJ.** Clinical applications of high-density surface EMG: a systematic review. *J Electromyogr Kinesiol* 16: 586–602, 2006. doi:10.1016/j.jelekin.2006.09.005.
44. **Farina D**, **Negro F**, **Gazzoni M**, **Enoka RM.** Detecting the unique representation of motor-unit action potentials in the surface electromyogram. *J Neurophysiol* 100: 1223–1233, 2008. doi:10.1152/jn.90219.2008.
45. **Farina D**, **Holobar A**, **Merletti R**, **Enoka RM.** Decoding the neural drive to muscles from the surface electromyogram. *Clin Neurophysiol* 121: 1616–1623, 2010. doi:10.1016/j.clinph.2009.10.040.
46. **Negro F**, **Muceli S**, **Castronovo AM**, **Holobar A**, **Farina D.** Multi-channel intramuscular and surface EMG decomposition by convolutive blind source separation. *J Neural Eng* 13: 026027, 2016. doi:10.1088/1741-2560/13/2/026027.
47. **Farina D**, **Cescon C**, **Negro F**, **Enoka RM.** Amplitude cancellation of motor-unit action potentials in the surface electromyogram can be estimated with spike-triggered averaging. *J Neurophysiol* 100: 431–440, 2008. doi:10.1152/jn.90365.2008.
48. **Bates D**, **Mächler M**, **Bolker B**, **Walker S.** Fitting linear mixed-effects models using lme4 (Preprint). *arXiv*, 2014. doi:10.48550/arXiv.1406.5823.
49. **Kuznetsova A**, **Brockhoff PB**, **Christensen RHB.** lmerTest package: tests in linear mixed effects models. *J Stat Soft* 82, 2017. doi:10.18637/jss.v082.i13.
50. **Lüdecke D**, **Ben-Shachar MS**, **Patil I**, **Waggoner P**, **Makowski D.** performance: An R package for assessment, comparison and testing of statistical models. *JOSS* 6: 3139, 2021. doi:10.21105/joss.03139.
51. **Lenth R**, **Singmann H**, **Love J**, **Buerkner P**, **Herve M.** emmeans: estimated marginal means, aka least-squares means (Online). 2020. https://CRAN.R-project.org/package=emmeans [2018 Dec 29].
52. **Genz A**, **Bretz F.** Comparison of methods for the computation of multivariate t probabilities. *Journal of Computational and Graphical Statistics* 11: 950–971, 2002. doi:10.1198/106186002394.
53. **Cohen J.** *Statistical Power Analysis For The Behavioral Sciences*. L. Erlbaum Associates; 1988.
54. **Rodriguez-Falces J**, **Place N.** Sarcolemmal excitability, M-wave changes, and conduction velocity during a sustained low-force

contraction. *Front Physiol* 12: 732624, 2021. doi:10.3389/fphys.2021.732624.
55. **Knikou M**, **Rymer WZ.** Hip angle induced modulation of H reflex amplitude, latency and duration in spinal cord injured humans. *Clin Neurophysiol* 113: 1698–1708, 2002. doi:10.1016/s1388-2457(02)00285-7.
56. **Gollnick PD**, **Sjödin B**, **Karlsson J**, **Jansson E**, **Saltin B.** Human soleus muscle: A comparison of fiber composition and enzyme activities with other leg muscles. *Pflugers Arch* 348: 247–255, 1974. doi:10.1007/BF00587415.
57. **Sweeney HL**, **Bowman BF**, **Stull JT.** Myosin light chain phosphorylation in vertebrate striated muscle: regulation and function. *Am J Physiol Cell Physiol* 264: C1085–C1095, 1993. doi:10.1152/ajpcell.1993.264.5.C1085.
58. **Vandenboom R**, **Grange RW**, **Houston ME.** Threshold for force potentiation associated with skeletal myosin phosphorylation. *Am J Physiol Cell Physiol* 265: C1456–C1462, 1993. doi:10.1152/ajpcell.1993.265.6.C1456.
59. **Lüscher HR**, **Ruenzel P**, **Henneman E.** Composite EPSPs in motoneurons of different sizes before and during PTP: implications for transmission failure and its relief in Ia projections. *J Neurophysiol* 49: 269–289, 1983. doi:10.1152/jn.1983.49.1.269.
60. **Clamann HP**, **Mathis J**, **Luscher HR.** Variance analysis of excitatory postsynaptic potentials in cat spinal motoneurons during posttetanic potentiation. *J Neurophysiol* 61: 403–416, 1989. doi:10.1152/jn.1989.61.2.403.
61. **Jackson A**, **Baker SN**, **Fetz EE.** Tests for presynaptic modulation of corticospinal terminals from peripheral afferents and pyramidal tract in the macaque. *J Physiol* 573: 107–120, 2006. doi:10.1113/jphysiol.2005.100537.
62. **Nielsen J**, **Petersen N.** Is presynaptic inhibition distributed to corticospinal fibres in man? *J Physiol* 477: 47–58, 1994. doi:10.1113/jphysiol.1994.sp020170.
63. **Burke D**, **Adams RW**, **Skuse NF.** The effects of voluntary contraction on the H reflex of human limb muscles. *Brain* 112: 417–433, 1989. doi:10.1093/brain/112.2.417.
64. **Proske U**, **Morgan DL.** Do cross-bridges contribute to the tension during stretch of passive muscle? *J Muscle Res Cell Motil* 20: 433–442, 1999. doi:10.1023/a:1005573625675.
65. **Proske U**, **Morgan DL**, **Gregory JE.** Thixotropy in skeletal muscle and in muscle spindles: a review. *Prog Neurobiol* 41: 705–721, 1993. doi:10.1016/0301-0082(93)90032-n.
66. **Gregory JE**, **Morgan DL**, **Proske U.** Aftereffects in the responses of cat muscle spindles. *J Neurophysiol* 56: 451–461, 1986. doi:10.1152/jn.1986.56.2.451.
67. **Wood SA**, **Gregory JE**, **Proske U.** The influence of muscle spindle discharge on the human H reflex and the monosynaptic reflex in the cat. *J Physiol* 497: 279–290, 1996. doi:10.1113/jphysiol.1996.sp021767.
68. **Inglis JG**, **Howard J**, **McIntosh K**, **Gabriel DA**, **Vandenboom R.** Decreased motor unit discharge rate in the potentiated human tibialis anterior muscle. *Acta Physiol (Oxf)* 201: 483–492, 2011. doi:10.1111/j.1748-1716.2010.02233.x.
69. **Klein CS**, **Ivanova TD**, **Rice CL**, **Garland SJ.** Motor unit discharge rate following twitch potentiation in human triceps brachii muscle. *Neurosci Lett* 316: 153–156, 2001. doi:10.1016/S0304-3940(01)02389-8.
70. **Vieira TM**, **Botter A.** The accurate assessment of muscle excitation requires the detection of multiple surface electromyograms. *Exerc Sport Sci Rev* 49: 23–34, 2021. doi:10.1249/JES.0000000000000240.
71. **McKiel A**, **Woods S**, **Gabriel DA**, **Vandenboom R**, **Falk B.** Post-activation potentiation and potentiated motor unit firing patterns in boys and men. *Eur J Appl Physiol* 124: 1561–1574, 2024. doi:10.1007/s00421-023-05377-z.
72. **Zero AM**, **Fanous J**, **Rice CL.** Acute and prolonged competing effects of activation history on human motor unit firing rates during contractile impairment and recovery. *J Physiol*. 601: 5689–5703, 2023. doi:10.1113/JP285189.
73. **Zero AM**, **Rice CL.** Without visual feedback voluntary torque is overestimated during muscle potentiation despite similar motor unit firing rate and perception of exertion. *J Neurophysiol* 133: 775–783, 2025. doi:10.1152/jn.00450.2024.
74. **Palmieri RM**, **Ingersoll CD**, **Hoffman MA.** The Hoffmann reflex: methodologic considerations and applications for use in sports medicine and athletic training research. *J Athl Train*. 39: 268–277, 2004.
75. **Soedirdjo SDH**, **Chung YC**, **Dhaher YY.** Sex hormone mediated change on flexion reflex. *Front Neurosci* 17: 1263756, 2023. doi:10.3389/fnins.2023.1263756.
76. **Hoffman M**, **Norcross M**, **Johnson S.** The Hoffmann reflex is different in men and women. *Neuroreport* 29: 314–316, 2018. doi:10.1097/WNR.0000000000000961.
77. **Rassier DE**, **Macintosh BR.** Coexistence of potentiation and fatigue in skeletal muscle. *Braz J Med Biol Res* 33: 499–508, 2000. doi:10.1590/s0100-879x2000000500003.
78. **Persechini A**, **Stull JT**, **Cooke R.** The effect of myosin phosphorylation on the contractile properties of skinned rabbit skeletal muscle fibers. *J Biol Chem* 260: 7951–7954, 1985. doi:10.1016/S0021-9258(17)39544-3.
79. **Sweeney HL**, **Stull JT.** Phosphorylation of myosin in permeabilized mammalian cardiac and skeletal muscle cells. *Am J Physiol Cell Physiol* 250: C657–C660, 1986. doi:10.1152/ajpcell.1986.250.4.C657.
80. **Westerblad H**, **Duty S**, **Allen DG.** Intracellular calcium concentration during low-frequency fatigue in isolated single fibers of mouse skeletal muscle. *J Appl Physiol (1985)* 75: 382–388, 1993. doi:10.1152/jappl.1993.75.1.382.
81. **Allen DG**, **Lannergren J**, **Westerblad H.** Muscle cell function during prolonged activity: cellular mechanisms of fatigue. *Exp Physiol* 80: 497–527, 1995. doi:10.1113/expphysiol.1995.sp003864.